

1 **Spatiotemporal dynamics during niche remodeling by super-**
2 **colonizing microbiota in the mammalian gut**

3
4 Guillaume Urtecho¹, Thomas Moody^{1,2}, Yiming Huang^{1,2}, Ravi U. Sheth^{1,2,3}, Miles Richardson^{1,2},
5 Hélène Descamps⁴, Andrew Kaufman¹, Opeyemi Lekan^{1,5}, Florencia Velez-Cortes^{1,2}, Yiming
6 Qu¹, Lucas Cohen¹, Deirdre Ricaurte^{1,2}, Travis E. Gibson^{6,7,8,9}, Georg K. Gerber^{6,7,10}, Christoph A.
7 Thaiss^{4,11,12}, & Harris H. Wang^{1,13,#}

8
9 ¹Department of Systems Biology, Columbia University, New York, NY, USA.
10 ²Integrated Program in Cellular, Molecular, and Biomedical Studies, Columbia University, New
11 York, NY, USA

12 ³Kingdom Supercultures, Brooklyn, NY, 11205 [current affiliation]

13 ⁴Department of Microbiology, Perelman School of Medicine, University of Pennsylvania,
14 Philadelphia, PA, USA

15 ⁵Columbia College, Columbia University, New York, NY 10027

16 ⁶Department of Pathology, Brigham and Women's Hospital, Boston, Massachusetts, USA

17 ⁷Harvard Medical School, Boston, Massachusetts, USA

18 ⁸Infectious Disease and Microbiome Program, Broad Institute, Cambridge, MA, USA

19 ⁹Computer Science and AI Lab, Massachusetts Institute of Technology, Cambridge, MA, USA

20 ¹⁰MIT-Harvard Health Sciences and Technology, Cambridge, Massachusetts, USA

21 ¹¹Institute for Diabetes, Obesity and Metabolism, Perelman School of Medicine, University of
22 Pennsylvania, Philadelphia, PA, USA

23 ¹²Institute for Immunology, Perelman School of Medicine, University of Pennsylvania,
24 Philadelphia, PA, USA

25 ¹³Department of Pathology and Cell Biology, Columbia University, New York, NY, USA.

26 [#]Correspondences should be addressed to harris.wang@columbia.edu.

27 **ABSTRACT**

28 While fecal microbiota transplantation (FMT) has been shown to be effective in reversing
29 gut dysbiosis, we lack an understanding for the fundamental processes underlying microbial
30 engraftment in the mammalian gut. Here, we explored a murine gut colonization model leveraging
31 natural inter-individual variations in gut microbiomes to elucidate the spatiotemporal dynamics of
32 FMT. We identified a natural ‘super-donor’ consortium that universally engrafts into diverse
33 recipients and resists reciprocal colonization. Temporal profiling of the gut microbiome showed
34 an ordered succession of rapid engraftment by early colonizers within 72 hours followed by a
35 slower emergence of late colonizers over 15-30 days. Moreover, engraftment was localized to
36 distinct compartments of the gastrointestinal tract in a species-specific manner. Spatial
37 metagenomic characterization suggested engraftment was mediated by simultaneous transfer of
38 spatially co-localizing species from the super-donor consortia. These results offer a mechanism
39 of super-donor colonization by which nutritional niches are expanded in a spatiotemporally-
40 dependent manner.

41 **INTRODUCTION**

42 The mammalian gut microbiome is composed of hundreds to thousands of bacterial
43 species that co-exist symbiotically with their host and provide key metabolic and protective
44 functions^{1–3}. Despite being subjected to the harsh gastrointestinal (GI) environment and
45 experiencing constant washout and nutritional shifts, the gut microbiome establishes reproducibly
46 across individuals during early development and eventually reaches an equilibrium by adulthood⁴.
47 Various environmental factors such as exposure to xenobiotics, antibiotics, or diet can lead to
48 altered microbiome compositions and increased susceptibility to colonization by pathogens and
49 pathobionts⁵. The recent success of fecal microbiota transplantation (FMT) to treat a disturbed
50 gut microbiome suggests a robust process by which a healthy microbiome can be restored⁶.
51 However, the detailed dynamics, mechanisms, and principles by which microbes successfully
52 engraft into a resident community remain unclear.

53 The stability and malleability of a microbiome is shaped by various ecological properties
54 including networks of inter-microbial interactions that manifest spatially and dynamically over
55 time^{7–9}. Metabolic interactions arise from commensal or mutualistic degradation of complex
56 substrates that support multiple species in a consortium^{10–12}. For example, *Bacteroides* in the gut
57 are known to excrete various carbohydrate degradation enzymes that in concert liberate different
58 sugars from dietary polysaccharides¹⁰. Similarly, diverse microbes spanning the length of the gut
59 participate in the deconjugation and step-wise biotransformation of host-secreted bile acids, which
60 alters local biochemical environments resulting in dramatic effects on gut biogeography¹³. Often,
61 these metabolic activities reinforce positive-feedback loops that gradually result in systemic
62 changes to the gut environment over sustained periods of time^{14,15,16}. Mapping these interspecies
63 interactions are key for assessing the stability of the microbiome and its susceptibility to
64 colonization by other microbes.

65 The ability to colonize and shape microbial communities by introducing foreign microbiota
66 is a quintessential goal of FMT therapies. Despite many successes, these therapies sometimes
67 exhibit mixed outcomes that vary between different combinations of donors and recipient^{17,18}.
68 Curiously, “super donors” that consistently engraft in a variety of recipients have been reported¹⁹.
69 While this phenomenon has been generally linked to species richness and diversity of donor
70 communities, it is currently unclear what specific mechanisms or determinants are
71 responsible^{18,20–23}. The maturation of these therapies is thus reliant on developing an
72 understanding of several key questions: Why do some strains engraft when others do not? Is
73 variability in engraftment success due to donor or recipient composition or are there other factors?
74 As the compositions of these microbial communities change, does their spatial structure change

75 to resemble the donor? Answering these questions will require effective models of FMT and
76 detailed dissection of the spatiotemporal dynamics and ecological interactions occurring within
77 the gut microbiome.

78 In this work, we use a murine model system that exploits natural variations in the gut
79 microbiome to study the temporal and spatial dynamics of microbial engraftment during FMT. This
80 model recapitulates key features of human FMT including recipient heterogeneity, temporal
81 successions, and diet dependencies while also providing tunable experimental parameters that
82 are difficult to control in human FMT trials. We show that microbiomes of C57BL/6 mice acquired
83 from different vendors exhibit variable outcomes when subject to pairwise FMT and identify a
84 “super donor” consortium. Transplantation and successful engraftment of distinct taxa within this
85 consortium occurred over short and long timescales. Further, we examine the spatial distribution
86 of microbial engraftment across the recipient GI tract and identify key genetic factors associated
87 with engraftment across different areas of the murine gut. Finally, spatial metagenomics was used
88 to study how the micron-scale spatial structure of microbial communities is affected by
89 engraftment, which revealed that spatial reorganization of the microbiota occurred concurrently
90 with altered metabolic capacities of the FMT recipient microbiome. These results introduce a
91 conceptual mechanism wherein colonizing microbes remodel metabolic niches temporally and
92 spatially within gut environments to facilitate microbial colonization.

93

94 RESULTS

95 A natural murine model of gut microbiome variability and diversity

96 To develop a robust murine model for FMT dynamics studies, we first explored whether
97 the murine gut microbiome exhibited the same degree of intra-host variability that is commonly
98 observed in human populations^{16,24}. Previous work suggested that genetically identical mice
99 sourced from different commercial vendors had distinct gut microbiota^{25–27}. To verify these
100 findings, we obtained conventional C57BL/6 mice from four different suppliers (Jackson Labs, J;
101 Taconic, T; Charles River, C; and Envigo, E) and performed 16S sequencing on their fecal matter
102 (**Figure 1A**). Indeed, we observed that the gut microbiome from different suppliers had
103 significantly distinct compositions in terms of taxa or OTUs (Operational Taxonomic Units) present
104 (PERMANOVA, $p = 0.001$) and differences in alpha diversity (**Figure 1B, S1A**). Mice from Envigo
105 displayed the greatest diversity, marked by high levels of *Prevotellaceae* and *Muribaculaceae*,
106 while Taconic mice had the lowest diversity with an elevated proportion of *Firmicutes* relative to
107 *Bacteroides* (**Figure S1B**). Importantly, the measured evenness of these mouse cohorts is within
108 range of what is observed between healthy human cohorts and those with gastrointestinal

109 disorders^{28,29} (**Figure S1C**). Therefore, the inter-vendor variability of the murine gut microbiome
110 may be a tractable surrogate model for studying the principles guiding microbiota transfer
111 between natural assemblages, which could help reveal shared properties underlying human FMT
112 engraftment and outcomes.

113

114 **Variable engraftment of gut microbiota in a murine model of FMT**

115 The inter-vendor variability in murine gut microbiomes is a useful property for an
116 experimental model of microbial gut colonization that mimics the process of FMT in humans^{30,31}.
117 We therefore aimed to implement a simple, yet robust protocol that does not require pre-
118 conditioning of the microbiome (e.g., use of antibiotics), and can leverage the natural variations
119 in gut microbiomes of otherwise genetically identical mice. It is well established that cohoused
120 mice from the same cage have nearly identical gut microbiomes because of fecal-oral
121 transmission via coprophagy^{30,32}. Leveraging this behavior, we cohoused mice from four different
122 suppliers in a pairwise manner and profiled their gut microbiota by fecal 16S sequencing before
123 (Day 0) and five days after (Day 5) cohousing (**Figure 1C**). Interestingly, we observed variable
124 outcomes in terms of the number of OTUs transferred between different pairs of mice (**Figure**
125 **1D**). In most cases, bi-directional transfer of taxa occurred between different mice, with the
126 number of unique OTUs transferred scaling linearly with the ratio of normalized entropy of the
127 donor microbiota (**Figure 1E**). Members of the Envigo microbiome, which exhibited the greatest
128 diversity, were capable of engraftment into all other microbiota and were highly resistant to
129 reciprocal colonization. Strikingly, a group of 23-33 Envigo OTUs effectively transferred to all
130 different recipient microbiota (**Figure S2**). Members of this “super-donor” consortium were
131 predominately of the *Muribaculaceae* family but also included other taxa, including
132 *Bacteroidaceae* and *Prevotellaceae* spp. (**Figure 1F**). While consistent sets of OTUs were
133 transferred from Envigo to all recipients, recipient-specific transfers were also observed, including
134 a pair of *Porphyromonadaceae* OTUs (OTU149 and OTU147) that were uniquely transferred to
135 Taconic mice. These observations suggest a robust but complex ecological process underlying
136 the observed colonization rather than random outcomes as predicted by the neutral theory of
137 community assemblages^{33,34}.

138 In addition to acquisition of new taxa, several OTUs initially present in the recipients were
139 displaced after exposure to the Envigo microbiota. Often, this displacement coincided with
140 transfer of phylogenetically related species from Envigo, which may indicate competition leading
141 to replacement within similar ecological niches. For instance, multiple Charles River
142 *Muribaculaceae* spp. (OTU60, OTU73, OTU184, OTU114) were displaced by ~18

143 *Muribaculaceae* spp. transferred from Envigo (**Figure 1F**). Similarly, native Jackson and Taconic
144 microbiomes contained high levels of single *Bacteroidaceae* spp. (OTU5 and OTU20,
145 respectively) which were depleted concurrently with transfer of Envigo *Bacteroidaceae*, (OTU9,
146 OTU14, OTU22, and OTU23). In other cases, native OTUs appear to be displaced in the absence
147 of any phylogenetically similar taxa present from Envigo. Taconic mice contained a distinct
148 population of 7 *Lachnospiraceae* OTUs (OTU139, OTU160, OTU174, OTU217, OTU240,
149 OTU271, OTU327) that decreased in abundance (Wilcoxon rank sum exact test, $p = 0.0006$) yet
150 no Envigo *Lachnospiraceae* were transferred. Therefore, Envigo microbiota appear to exhibit a
151 “super-donor” phenotype that is sometimes observed in human FMT trials²². Recalcitrance of
152 Envigo microbiota to invasion or displacement by other microbiota highlights this dominant
153 persistence and colonization resistance phenotype.

154

155 **Ordered temporal microbiota transfer during murine FMT**

156 To better elucidate the temporal dynamics of microbial transfer during our FMT model, we
157 performed fecal 16S profiling of Jackson (Jax) mice cohoused with Envigo (Env) mice over 32
158 days. The Jax-Env pairing was chosen because they had significant differences in gut microbiome
159 diversity ($p = 0.00032$, Wilcoxon rank sum test, **Figure 1B**). Beyond the dramatic changes to the
160 Jax microbiome after five days of cohousing with Env mice, we were surprised to find that the
161 microbiome of these recipient Jax mice (Jax^{Env}) continued to change weeks after initiation of
162 cohousing (**Figure 2A**). Microbes transferred to Jax^{Env} mice within the first five days were mostly
163 *Lactobacillaceae* and *Muribaculaceae* whereas *Lachnospiraceae* emerged and reached
164 moderate relative abundance over the latter half of this time-course experiment. Interestingly, Env
165 *Lachnospiraceae* only began to colonize after 15 days, coinciding with the depletion of Jax
166 *Lachnospiraceae*, which may suggest these incoming species are able to take advantage of a
167 *Lachnospiraceae*-specific niche once it is vacated. Overall, differential abundance analysis
168 showed 31 unique OTUs engrafted into Jax^{Env} mice, with 21 (67.7%) of these transferring within
169 the first five days of cohousing (**Figures 2B, 2C**). At the conclusion of this time course, the Jax^{Env}
170 microbiome exhibited higher population diversity and clustered more closely with the Env
171 microbiome based on Principal Component Analysis (PCA) (**Figure S3A, S3B**). As controls,
172 cohoused cage mates from the same vendor (i.e., Jax^{WT} or Env^{WT}) did not lead to notable changes
173 in the gut microbiome, nor did the recalcitrant Env mice when exposed to Jax microbiota (i.e.,
174 Env^{Jax}) (**Figure S3C, Figure S3D**). These results show that transplanted microbiota emerge over
175 both short (days) and long (weeks) time scales, which may indicate a gradual transition in the gut
176 milieu towards stabilization.

177 Stable engraftment of new OTUs could correspond to expansion of niches in the gut, which
178 would be reflected by an increase in carrying capacity of the community. We therefore assessed
179 changes in bacterial density throughout FMT using absolute abundance measurements of fecal
180 samples (Methods). Despite the consistent increase in unique OTUs observed over time,
181 population load exhibited substantial temporal fluctuations. Overall biomass decreased over the
182 first two days before a dramatic expansion followed by an equilibration (**Figure 2D**). By Day 30
183 the relative biomass corresponding to taxa specific to the Jax microbiota was entirely replaced by
184 Env taxa in Jax^{Env} mice. While Env^{Jax} mice also experienced a bottleneck in population size at
185 Day 2, there was no dramatic increase in biomass and the microbiome ultimately reverted to its
186 original state. Neither control groups showed this phenomenon (**Figure S3E**). Our data therefore
187 suggests that the convergence of microbial communities during FMT results from a transitionary
188 state with a rapid and dramatic interval of population bottlenecking, followed by restructuring and
189 re-equilibration of the new community.

190

191 **Microbial transplantation dynamics vary across murine gut compartments**

192 The mammalian gut contains many ecological niches whose diverse environmental,
193 biochemical, and ecological properties shape the gut biogeography, resulting in distinct microbial
194 populations across different gut compartments³⁵. Therefore, analysis of fecal pellets gives an
195 incomplete picture of all changes occurring along the intestinal tract since fecal matter
196 predominantly reflects the distal gut^{36–38}. To explore engraftment dynamics across different
197 compartments along the murine intestinal tract following FMT, we obtained GI samples upon
198 necropsy at the conclusion of the 32-day Env-Jax cohousing experiment and performed 16S
199 profiling of individual gut compartments spanning the entire intestinal tract (**Figure 3A**). PCA
200 showed that the OTU composition of Jax^{Env} was more similar to that of Env across all gut
201 compartments (**Figure S4A**). Interestingly, the taxonomic composition of the Jax microbiome
202 appeared to be more uniform across gut compartments, whereas the gut microbiomes of Env^{WT}
203 and Jax^{Env} cohorts were more stratified, with distinct microbial profiles in the small and large
204 intestines. We confirmed this by performing an Analysis of Similarities³⁹ (ANOSIM) and found that
205 Jax gut compartments were significantly less dissimilar to each other than Env^{WT} or Jax^{Env}
206 compartments (**Figure S4B**). Ultimately, FMT resulted in population remodeling across the entire
207 length of the GI tract, shifting the 16S microbiome profiles of Jax^{Env} mice to resemble the Env
208 microbiome across all gut compartments.

209 To quantitatively assess how overall microbial communities were affected across different
210 sections of the GI tract, we looked at changes in the biomass of different taxonomic groups in

211 these areas. The composition of engrafting microbes varied dramatically across different
212 compartments. Five species of Env-specific *Lactobacillaceae* were the primary colonizers of the
213 small intestine, whereas diverse populations including *Muribaculaceae*, *Prevotellaceae*, and
214 *Lactobacillaceae* colonized the cecum and colon of Jax^{Env} mice (**Figure 3B**). Conversely, a
215 majority of the Jax recipient-specific biomass was displaced, especially within upper-GI
216 compartments where overall bacterial biomass decreased by as much as 97.2% in the duodenum
217 (**Figure 3C**). As was observed in our longitudinal profiling, OTUs specific to the Jax microbiome
218 were nearly entirely replaced across all gut compartments while a proportion of the microbial taxa
219 shared between the Env donor and Jax^{Env} decreased from 85-70% to 15-30% of the population
220 of each gut compartment (**Figure 3D**). These data reflect the highly variable effects of FMT on
221 microbial biomass and composition between intestinal compartments in the recipient.

222 Next, we explored whether the timing of ‘early’ or ‘late’ colonizing species was related to
223 the areas they colonized in the gut. We compared the distribution of microbes to the order they
224 colonized the GI tract observed in our longitudinal study (**Figure S4C**). Interestingly, “early
225 colonizing” bacteria (mainly *Lactobacillaceae*) were more commonly observed in the upper GI
226 whereas “late colonizers” were relatively enriched in the cecum and colon. Late-colonizing
227 species nearly exclusively consisted of *Muribaculaceae* and *Lachnospiraceae*, the abundance of
228 which are positively correlated with microbial production of deoxycholic acid (DCA)⁴⁰. Considering
229 conversion of primary bile acids to DCA is predominately facilitated by microbes in the upper GI⁴¹,
230 early colonizing microbes may gradually alter DCA levels, enabling colonization by
231 *Lachnospiraceae*. This raises the possibility that the late colonization phenomenon is due to early
232 colonizers changing the biochemical properties of the gut before conditions are permissive to late
233 colonizers.

234 In addition to engraftment of Env bacteria, the spatial distribution of many OTUs already
235 found in Jax mice changed across the gut (**Figure 3E**). In some cases, these OTUs were
236 consistently depleted across all gut compartments (OTU10, OTU52) whereas other microbes
237 appeared to have been selectively depleted in specific gut compartments, but not others. The
238 abundance of *Duncaniella* OTU4 decreased by 2-3 orders of magnitude in the small intestines
239 yet remained unchanged in the colon. Similarly, OTU138, a *Bifidobacterium*, was found across all
240 gut compartments in Jax mice, yet became restricted to the cecum in Jax^{Env} mice. This shows
241 that microbial transfer by FMT results in non-uniform colonization across different areas of the gut
242 and alters the biogeography of native species.

243

244 **FMT outcomes reflect micron-scale spatial structuring of OTUs within recipient and donor
245 communities**

246 The gut microbiome exhibits local spatial structuring that reflects complex inter-microbial
247 interactions driven by mutualistic, commensal, and competitive processes⁴². Given the dramatic
248 changes to the microbiome of Jax recipients following FMT from Env donors (i.e., Jax^{Env}), we
249 characterized the changes to the spatial structure of the microbiome using MaPS-seq, a
250 sequencing-based method recently developed in our lab to obtain micron-scale species spatial
251 co-association information⁴³. We compared the microbial spatial co-association from Jax^{Env} with
252 that of the Env^{WT} and the Jax^{WT} controls (N = 4 each) before and after 32 days of cohousing. In
253 total, 20,992 unique MaPS-seq particles (20-40 µm in diameter) were profiled to reconstruct the
254 spatial organization across these animal cohorts.

255 First, we sought to identify spatial co-associations between taxa pairs. A frequentist
256 approach was used to simulate the co-occurrence of two OTUs within particles by generating the
257 null distribution of co-occurrences for all pairs of OTUs, and then determining which microbes co-
258 occurred within particles significantly more or less frequently than expected by chance⁴⁴. This
259 analysis evaluated spatial co-associations between 7,430 microbial pairs and identified 292
260 statistically significant co-associated OTU pairs from the Jax^{WT} microbiome (adjusted p < 0.05,
261 randomization test) and 494 in Env^{WT} (**Figure S5**). Hierarchical clustering of these co-association
262 pairs revealed distinct groupings. In Jax^{WT}, spatial associations were predominately found
263 amongst *Clostridia* species and separated into four distinct groups (**Figure 4A**). Groups 1 and 4
264 formed highly connected within-group co-associations. Groups 2 and 3 had less within-group co-
265 associations, except for a few strongly co-localized OTU pairs (e.g., Group 2: OTUs 79 and 56,
266 Group 3: OTUs 148, 27, 5, and 99). Interestingly, we detected strong anti-associations between
267 Groups 1 and 4; some Group 3 members also had negative association with members of Groups
268 1 and 4, suggesting spatial segregation across groups. In Env^{WT}, we also observed four main
269 groups of co-associated taxa (**Figure 4B**). Group 1 was distinctly dominated by *Clostridia* species
270 and exhibited negative co-associations with *Bacteroidia* communities found in Groups 2 and 4. In
271 contrast, Group 4 displayed the most class-level diversity, containing a mix of *Clostridia*,
272 *Bacteroidia*, and *Bacilli*; this group had negative associations with Group 2, which was primarily
273 composed of highly co-associated *Bacteroidia*. Lastly, Group 3 also consisted mainly of
274 *Bacteroidia*, albeit with weaker overall interactions compared to other *Bacteroidia*-centric
275 communities. These distinct spatial co-localizations suggest an organized community structure in
276 the Env^{WT} and Jax^{WT} microbiomes of ecologically segregated *Clostridia* and *Bacteroidia* taxa.

277 We then analyzed the Jax^{Env} microbiota to explore how spatial patterns can be altered
278 following FMT (**Figure 4C**). In general, Jax^{Env} particles contained significantly more distinct OTUs
279 per particle than Jax^{WT} particles (Jax^{Env}: 3.76, Jax^{WT}: 2.88, $p < 2 \times 10^{-16}$, Wilcoxon rank-sum test),
280 indicating Env microbiota transfer into to the Jax community moderately increased species
281 richness at the micrometer scale (**Figure S6**). We detected 499 significant spatial co-associations
282 in Jax^{Env} that clustered into four groups (**Figure 4C, Figure S5**). While the Jax^{Env} microbiota was
283 mostly comprised of Env OTUs, numerous *Clostridia* Jax OTUs were retained. Fascinatingly,
284 some transferred Env OTUs reassembled into a spatial structure resembling their same
285 configuration in the original Env^{WT} microbiota whereas others formed hybrid communities with Jax
286 taxa. In Group 1, *Bacteroidia* species reunited within the recipient microbiome creating a
287 community exclusively consisting of Env OTUs. This group exhibited intriguing relational
288 dynamics: it had positive associations with Group 2, but a mixture of strongly negative and positive
289 interactions with Group 4. Overall, Group 2 exhibited relatively weak spatial structuring aside from
290 a strongly positive co-association between OTU30 and OTU96. Interestingly, this association was
291 also observed in the Jax^{WT}, and was preserved through FMT. Group 3 was driven by a particularly
292 strong co-associations between an Env *Bacilli* (OTU15) and Jax *Erysipelotrichia* (OTU5) and
293 these taxa were negatively associated with nearly all other members of the microbiome.
294 Intriguingly, in Env^{WT}, OTU5 formed strong spatial association with another *Erysipelotrichia*
295 (OTU7) (**Figure 4B**). Not only did OTU15 form a strong association with the Jax OTU5, but it also
296 became negatively associated with its Env^{WT} partner, OTU7. This observation highlights the
297 dynamic ecological strategies microbes can employ to successfully adapt and colonize in the
298 context of FMT.

299 We then explored whether microbes transferred by FMT retained their spatial groups
300 through the transfer from the original microbiomes to Jax^{Env} (**Figure 4D**). Flow analysis
301 demonstrated that while a fraction of each spatial group was preserved through transplantation,
302 donor microbes predominantly formed novel subcommunities within the recipient gut
303 environment. Spatial groups appeared to cluster more by their taxonomic composition than by
304 their original group, indicating that taxonomic identity plays a more decisive role in the formation
305 and stabilization of new microbial communities following transplantation. Jax^{Env} Group 1 was a
306 hybrid community of *Bacteroidia* derived from multiple Env^{WT} groups, particularly those from Env
307 Groups 2 and 3. Jax^{Env} Group 2 received the largest share of Jax taxa, most of which were co-
308 associated before FMT in the Jax^{WT} Group 4. Intriguingly, all constituents of Env Group 2, which
309 exhibited the most robust associations in Env^{WT}, achieved successful transfer.

Considering this observation, we examined whether the presence of spatial associations in the donor microbiome was predictive of FMT outcomes in the recipient. Indeed, the number of spatial associations by Env microbes in their Env^{WT} native microbiome was correlated to their engraftment success in the Jax^{Env} recipient ($R^2 = 0.61$, $p = 3.7 \times 10^{-12}$) (**Figure 4E**). Amongst Jax taxa, microbes with the most interactions in Jax^{WT} were not necessarily more stable post-FMT. Rather, Jax microbes that remained stable following FMT were found to increase in the number of associations they exhibited in Jax^{Env} and these new associations were formed with Env taxa (**Figures S7**). Furthermore, bacteria significantly enriched in Jax^{Env} compared to Jax^{WT} had notably more spatial associations than microbes with either unchanged abundance ($p = 9.4 \times 10^{-15}$, Wilcoxon rank sum test) or those depleted after FMT ($p = 1.5 \times 10^{-7}$, Wilcoxon rank sum test) (**Figure 4F**). Altogether, these results suggest microbes with the capacity to form spatially organized communities are better able to engraft compared to species that do not.

322

323 **Exploitation of open nutritional niches as a key determinant of FMT engraftment success**

We hypothesized that the successful engraftment of spatially associated communities is facilitated by enhanced metabolic capabilities, enabled by synergistic mutualistic interactions such as cross-feeding. To catalog the metabolic diversity across mice gut microbiomes from different suppliers, we performed shotgun metagenomic sequencing on their fecal DNA, which yielded a 240 Gigabase (Gb) dataset that assembled into 457 metagenome-assembled genomes (MAGs) with annotated gene functions (Methods). Rather than relying on existing mouse strain databases, we performed *de novo* assembly to avoid database biases favoring different vendors or culturable strains. This collection of MAGs covers over 80% of all genus-level diversity across the four distinct C57BL/6 gut microbiomes (**Fig 5A, Table S1**). Upon taxonomically assigning MAGs, we confirmed that Envigo consortia harbored a higher number of *Muribaculaceae*, 35 distinct MAGs, which are known to be prolific mucin foragers with diverse polysaccharide degradative capacities²⁹. More detailed genomic characterization (Methods) of the Carbohydrate-Active Enzyme (CAZyme) repertoire within *Muribaculaceae* MAGs revealed that these microbes contained a set of unique CAZyme families (GH148, GH155, GH158, GH121, GH116, GH47), which may indicate these bacteria are able to utilize a broader range of dietary polysaccharides (**Figure 5B, Methods**). Beyond CAZyme differences, we investigated whether certain KEGG pathways were enriched between these metagenomes but did not find any significant differences (**Figure S8A**). These findings highlight that the mouse gut microbiomes derived from different vendors exhibit distinct microbial profiles and variability in CAZyme composition, which may lead to differences in polysaccharide utilization between these cohorts.

344 Given that the most prolific colonizers in the Env microbiota consisted of spatially
345 organized *Bacteroidia* communities, we sought to explore how Jax and Env *Bacteroidales*
346 communities differed in their metabolic capacities to access nutrient niches in the gut
347 environment. *Bacteroidales* are the primary metabolizers of complex dietary polysaccharides in
348 the gut and work in concert to break down these macromolecules into consumable subunits¹⁰.
349 Interestingly, gut colonization of engineered probiotics can be enhanced by fiber supplementation,
350 in cases where the probiotic is the sole species capable of metabolizing that fiber^{45,46}. Therefore,
351 we hypothesized that the super-colonizing phenotype of Env *Bacteroidia* is driven by their ability
352 to metabolize previously inaccessible dietary fibers within the Jax recipient GI tract.

353 We evaluated the abilities of fecal communities from Env^{WT}, Jax^{WT}, and Jax^{Env} mice to
354 utilize various complex polysaccharides. Growth assays on fecal communities was performed
355 over 48 hours using defined minimal media supplemented with a panel of simple and complex
356 carbohydrates to characterize the range of accessible polysaccharides. Growth is only possible if
357 the community can break down the supplemented complex polysaccharides. We observed
358 striking differences in growth profiles between the microbiomes. Env^{WT} and Jax^{Env} microbiota
359 could utilize certain complex dietary polysaccharides (e.g., inulin, cellobiose) as the sole carbon
360 source while Jax^{WT} microbiota could not (**Figure 5C**). Moreover, the complex modified gifu
361 anaerobic media (mGAM) could support growth of Env^{WT} and Jax^{Env} but not Jax^{WT} microbiota.
362 Conversely, the native Jax^{WT} microbiota grew faster in glucose, arabinan, and arabinogalactan
363 indicating specialization for using these resources. 16S profiling of saturated communities showed
364 that more diverse *Bacteroidales*-enriched populations grew from the Env^{WT} and Jax^{Env}
365 communities in all conditions (**Figure S8B**). This is consistent with the idea that mixed
366 communities of engrafted *Bacteroidales* work cooperatively to break down previously unused
367 dietary polysaccharides into available carbohydrates. This data therefore suggest that the Env
368 microbiome can access a broader set of carbohydrate nutrients to supplement their growth, which
369 allow them to exploit unfilled nutrient niches in the recipient Jax gut microbiota. FMT from Env
370 microbiota imparts the ability for this ecosystem to metabolize additional carbohydrates, which
371 may expand the accessible nutrient niches within the recipient gut and increase the carrying
372 capacity of the environment.

373

374 **Using humanized mouse gut microbiomes to simulate human FMT outcomes**

375 Finally, we explored the use of our murine model to simulate FMT dynamics between
376 humans. Notably, the humanized mouse model allows the study of reciprocal FMT between two
377 microbiomes which is not practically feasible in human FMT studies. We acquired fecal samples

378 from three representative human donors of the three major human gut microbiome enterotypes⁴⁷.
379 These individuals, H1, H3, and H5, were dominated by *Ruminococcaceae* (enterotype 3),
380 *Prevotellaceae* (enterotype 2), and *Bacteroidaceae* (enterotype 1), respectively. We gavaged
381 germ-free mice with these fecal samples and observed engraftment after nine days that only
382 partially resembled their respective human donors (**Figure S9A**). Humanized mice were
383 predominately colonized by families *Bacteroidaceae* and *Akkermansiaceae* regardless of the
384 enterotype of the donor, whereas *Prevotellaceae* and *Ruminococcaceae* were poorly
385 represented. Moreover, the microbiomes of humanized mice were similar at the family-level but
386 varied greatly when comparing OTU-level resolution and diversity metrics (**Figure S9B**). Although
387 humanized mice microbiomes did not fully recapitulate the microbiomes of their donors⁴⁸, PCA
388 showed the greatest similarity to their respective donors (**Figure S9C**). We then performed
389 pairwise co-housing between humanized mice to explore FMT outcomes between human
390 microbiomes (**Figure 6A**). After nine days of cohousing, fecal 16S sequencing revealed two main
391 groups of microbes that exhibited similar transfer dynamics and were generally enriched for
392 members of the order *Clostridiales* (**Figure 6B**). PCA showed that when M5 mice were cohoused
393 with M1 or M3 mice (i.e., M5^{M1}, M5^{M3}) the M5 microbiome composition shifted to resemble the
394 other microbiomes (**Figure 6C**). On the other hand, cohoused M1^{M3} & M3^{M1} mice form a new
395 grouping resembling an intermediate between M1^{WT} and M3^{WT}. Examining the number of OTUs
396 transferred, we found M1 and M3 mice transferred 30 and 26 species to M5 mice, and these
397 OTUs were predominately *Clostridiales* (**Figure 6D**). The large number of *Clostridiales* transferred
398 to M5 mice is notable given that the M5 mouse microbiome contained the fewest number of
399 *Clostridiales* OTUs (**Figure S9D**). Therefore, this may indicate the M5 microbiomes contained a
400 vacancy in *Clostridiales* niches that were exploited to promote engraftment of additional *Clostridia*
401 and that the taxonomic ‘completeness’ of a microbiome may determine permissiveness to
402 engraftment. This is consistent with the results of a recent meta-analysis of FMTs that showed
403 community-dissimilarity between donor and recipient was a strong predictor of engraftment²³.
404 Overall, these results show that humanized murine gut models produce interesting FMT outcomes
405 that could provide further insights into the determinants of microbiota transfer and colonization in
406 humans.

407

408 DISCUSSION

409 In this study, we characterized microbial gut colonization in a murine FMT model that
410 exploited natural microbiota variations in different mouse cohorts. Through pairwise co-housing
411 and FMT experiments, we identified a “super donor” microbiome from Envigo mice suppliers

412 capable of dominantly engrafting into other murine microbiomes and reciprocally resisting
413 colonization by all other microbiomes. Longitudinal profiling of a Env-Jax FMT pair revealed
414 kinetics of colonization and adaptation of the microbiome in Jax^{Env} groups, characterized by
415 immediate and gradual engraftment and multiple surges in microbiota abundances. Spatially
416 characterizing the microbiota across different GI compartment showed that Env and Jax^{Env} mice
417 had similarly more segregated microbial populations across the GI tract than compared to Jax
418 mice. Application of MaPS-seq to these microbiome samples showed these microbiomes contain
419 spatially separated communities that transfer collectively but reorganize in the recipient during
420 FMT. Finally, a humanized gut microbiome FMT experiment demonstrated the utility of this murine
421 model for studying FMT potential between human cohorts.

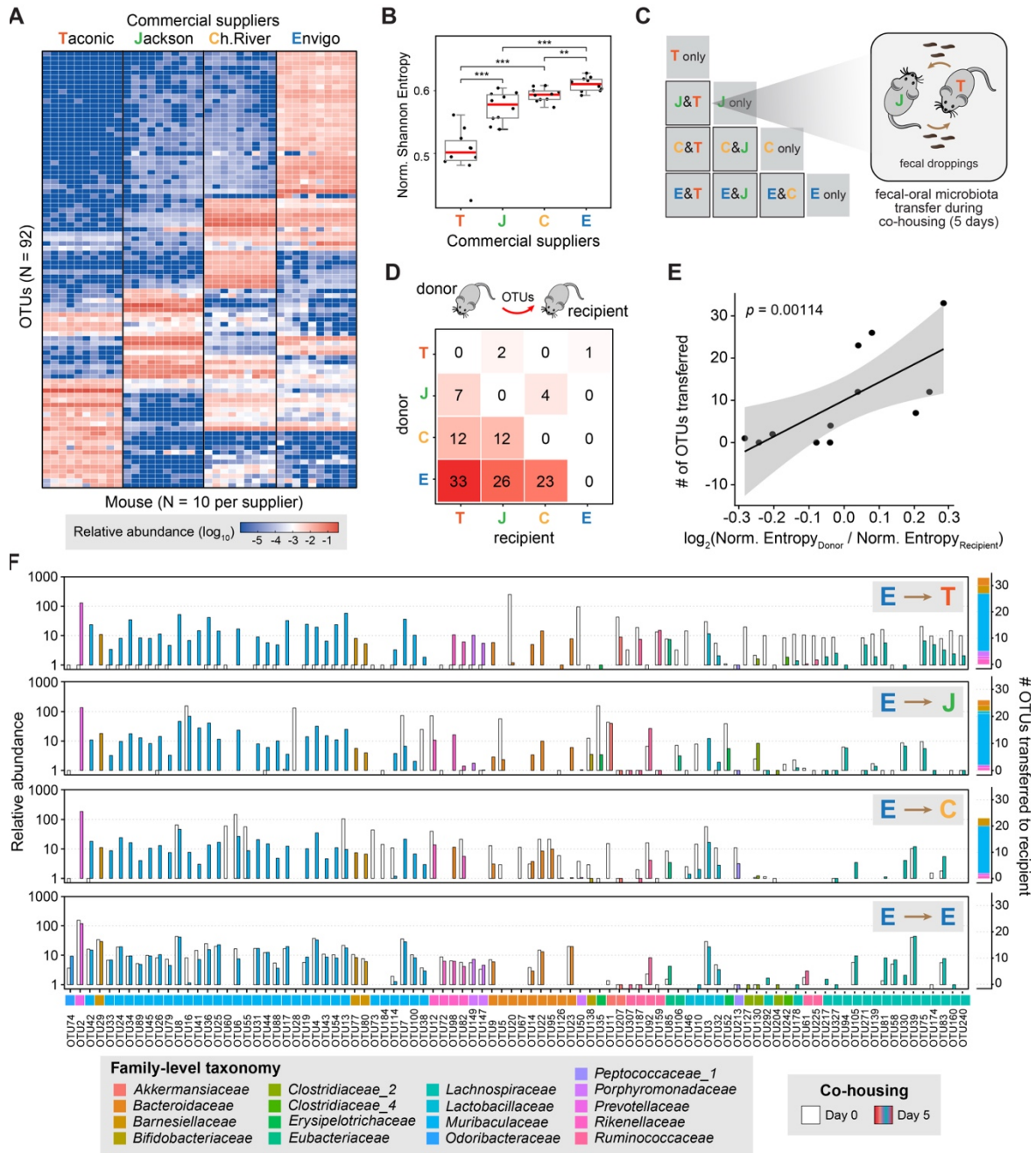
422 Our observations highlight several key features underlying bacterial engraftment in the
423 gut. Through kinetic studies, we found both short (days) and long (weeks) timescale emergence
424 of transferred strains. We hypothesize that following initial FMT, microbes begin a gradual process
425 of shaping the gut environment such that native taxa are suppressed, which ultimately paves the
426 way for other transferred species to gain a foothold. This may occur due to changing of the
427 biochemical properties or by the suppression of native species. Thus, the temporal dynamics and
428 succession observed during FMT may mirror those seen in other examples of microbial
429 colonization, such as following antibiotics or development^{49–51[cite]}. Future studies should examine
430 the metabolic and biochemical changes that occur during this process, which may reveal new
431 facets about how microbial communities interact and are established. A particularly interesting
432 observation from this temporal analysis was the sharp drop in overall microbial population load in
433 the short-term following FMT followed by a bloom and subsequent stabilization. This observation
434 may be explained by the results of a previous longitudinal study, which showed that dramatic
435 microbial community transitions are often preceded by an initial population-level bottleneck before
436 dense, stable communities are established⁵². This may be a general phenomenon that occurs
437 during the merging of microbial communities and warrants further investigation to learn the inter-
438 microbial dynamics responsible, which may include direct antagonism or the collapse of cross-
439 feeding networks.

440 Using MaPS-seq, we showed for the first time the micron-scale consequences of FMT on
441 communities within a recipient gut. This analysis revealed a key observation that microbes form
442 spatially associated communities in the gut and these communities are reassembled in the
443 recipient during FMT. Furthermore, these units may actively displace other native community units
444 found in the recipient. Generally speaking, microbes exhibiting the greatest number of spatial
445 associations in the donor microbiome were more successful at colonizing the recipient GI tract

446 than those that do not. Given that spatial relationships may represent underlying ecological
447 interactions, such as mutualism, cooperation, or competition, these spatial associations may
448 provide crucial information for understanding the inter-species mechanisms affecting how
449 microbial communities are established during FMT.

450 In this study, a positively co-associating group of *Bacteroidia* was found to transfer from
451 Envigo donors to Jax recipients. Further functional studies in defined media showed that the Env
452 microbiota are capable of broadly utilizing polysaccharides that are otherwise inaccessible to the
453 Jax microbiota. While Jax microbes were capable of metabolizing fewer carbohydrates, they grew
454 faster than Env microbes when provided appropriate resources, suggesting more of a specialist
455 than generalist lifestyle. We speculate that the trade-off of generalist versus specialist
456 communities may be an important factor in determining the success of FMT therapies and that
457 generalist communities may be better suited for engraftment into recipients. Given that the
458 mammalian intestinal tract is a dynamic environment, with constantly fluctuating resources and
459 host-derived inputs⁵³⁵⁴, generalists may be more effective at enduring these changing conditions
460 and ultimately supplanting populations of specialists. Indeed, generalist communities have been
461 found to outperform specialists during the merging of aquatic microbial communities under
462 dynamically changing environmental conditions⁵⁵. Another explanation for the success of
463 generalist communities is that the broad range of nutrients they can utilize equips them to exploit
464 unused nutritional niches within recipient gut environments as metabolically independent units⁵⁶.
465 The creation of nutritional niches through dietary supplementation has shown to be an effective
466 tool for enabling engraftment of probiotic microbes^{45,57}. However, our research reveals that
467 unused niches in the recipient gut environment may be exploited to promote the successful
468 transplantation of microbiota into the mammalian gastrointestinal tract.

469 This work systematically explored the spatiotemporal dynamics of microbial colonization
470 following FMT. Future applications of this approach could better delineate the role of host-factors
471 in FMT outcomes and under clinically relevant settings such as exposures to antibiotics and
472 xenobiotics. Ultimately, we expect more detailed spatial, temporal, genomic, and metabolic
473 characterizations of the gut microbiome FMT kinetics will lead to more predictive FMT models
474 that can unlock the true potential of this microbiome manipulation approach for a variety of clinical
475 applications.



476

477 **Figure 1. Diverse murine gut microbiomes exhibit variable outcomes to pairwise FMT (A)** Microbiome
 478 composition of BL57BL/6 mice sourced from four vendors by 16S rRNA sequencing (N = 10 mice / vendor). **(B)** Shannon diversity index of mouse microbiomes (N = 10, Wilcoxon rank-sum test, *** = $p < .001$). **(C)**
 479 Pairwise fecal microbiota transfer (FMT) model by cohousing female C57BL/6 mice from different vendors.
 480 **(D)** Number of OTUs transferred between mice from different vendors. **(E)** The number of OTUs transferred
 481 from donor to recipient correlates with the ratio of their normalized Shannon Entropies. **(F)** (left) Relative
 482 abundance of OTUs at Day 0 and Day 5 of cohousing with Envigo mice. OTUs are ordered by Phylogenetic
 483 distance(right). Number and taxonomic identity of OTUs transferred from Envigo microbiome to various
 484 recipients.

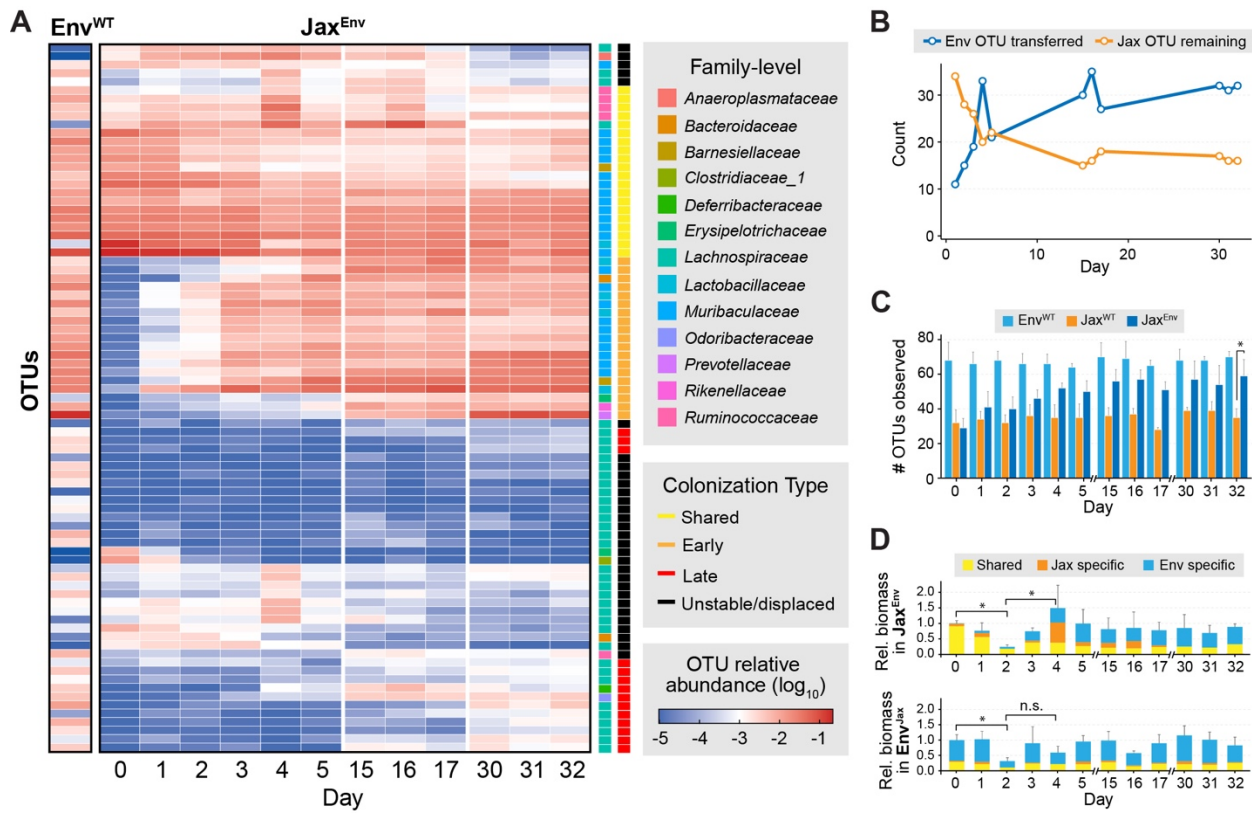
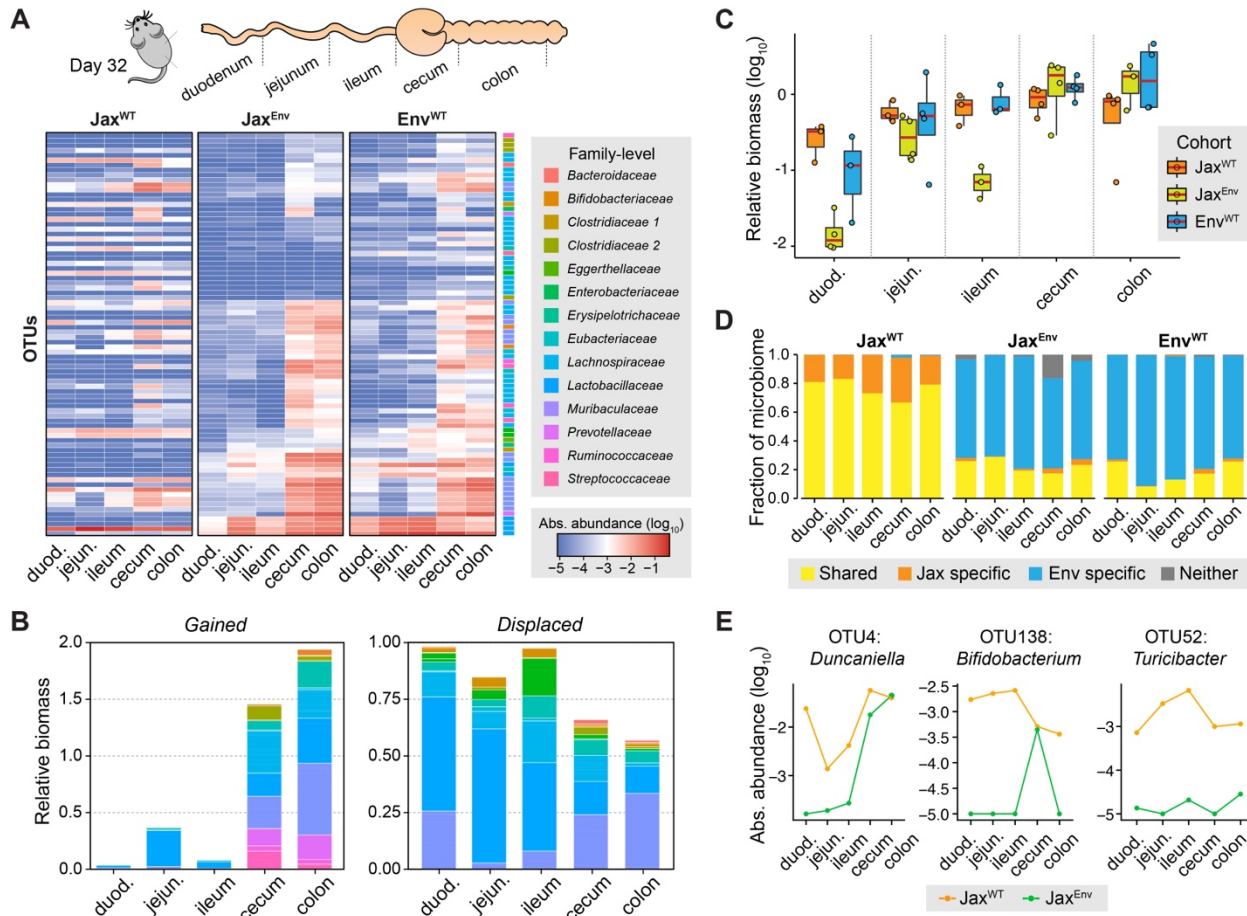
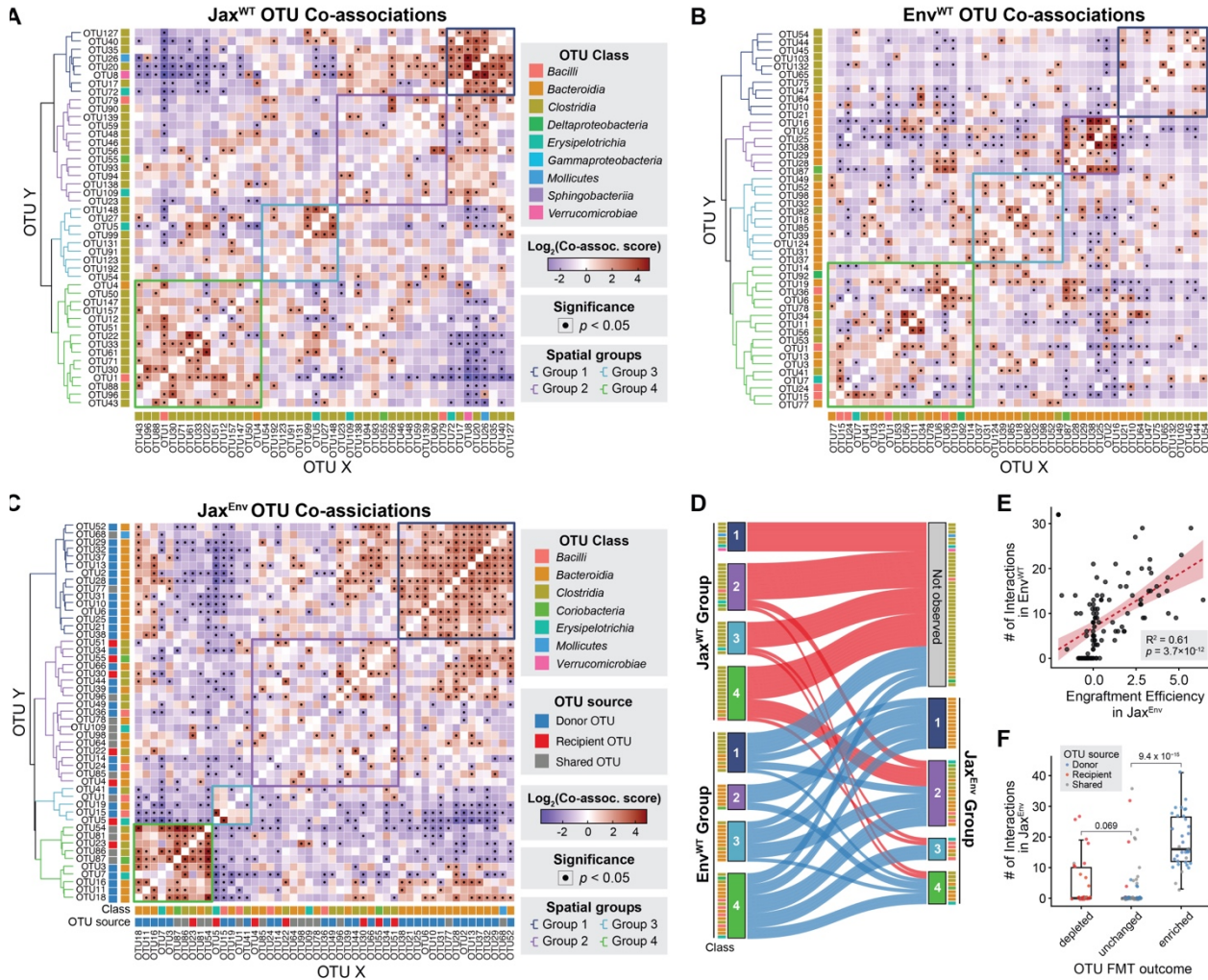


Figure 2. The transfer of microbes by FMT occurs over short and long-time scales. (A)
 Longitudinal 16S microbiome profiling of Jax^{Env} mice (N = 5). Detectable colonization by transferred OTUs occurs during both early (days 1-5) and late (days 15-32) sampling points.
(B) Representative Envigo microbiome is an average of day 1 Env-Env cohoused mice (N = 5). Number of Env OTUs transferred and Jax OTUs remaining over longitudinal sampling. **(C)** Number of OTUs detected over time within each mouse cohort. We observed a significant increase in the number of OTUs present within Jax^{Env} mice compared to Jax^{WT} after 32 days of cohousing (Wilcoxon rank sum test, $p = 0.029$, n = 4). **(D)** Changes in bacterial biomass within feces of Jax^{Env} and Env^{Jax} mice. Biomass is colored by whether OTUs are uniquely found in microbiomes of Envigo donors (Donor specific), uniquely found in Jackson Recipients (Recipient specific), or observed in both. Values normalized to Day 0 of cohousing (* = $p < 0.05$, one-sided Wilcoxon rank sum test).

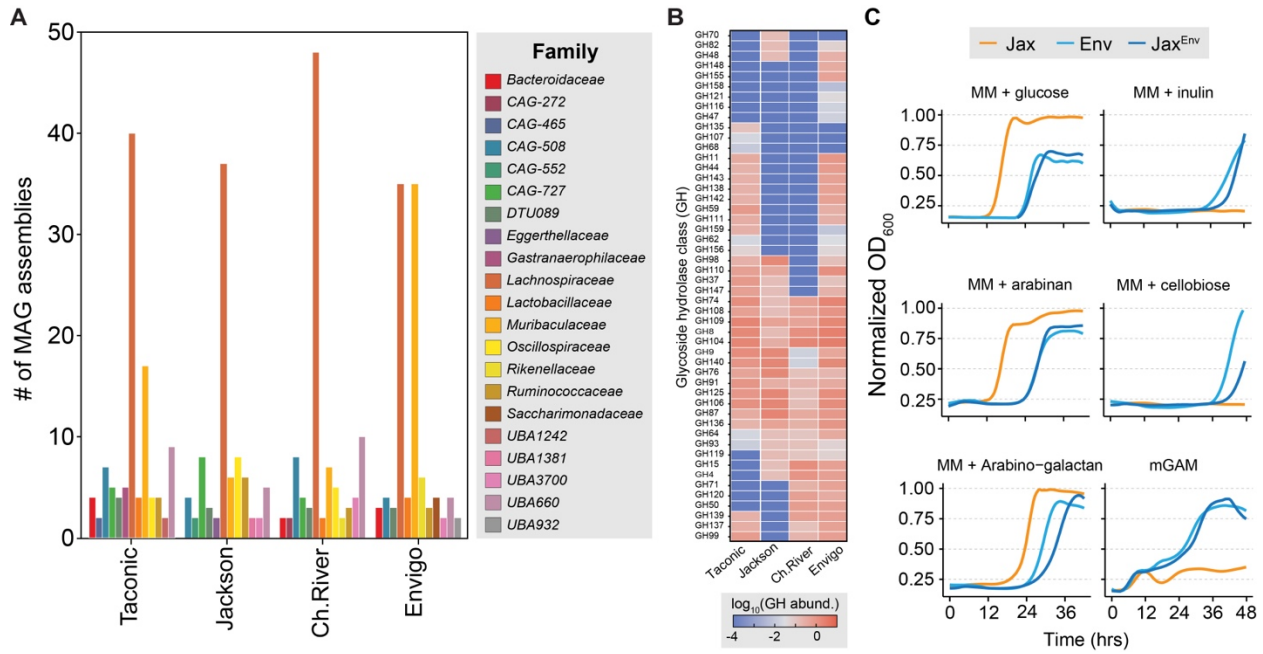


502
503 **Figure 3. Microbial transplantation dynamics vary across murine gut compartments. (A)**
504 16S profiling of luminal contents of mice cohorts after 32 days of cohousing. Rows are arranged
505 by hierarchical clustering (Euclidean distance, Complete Linkage) of cohoused Jackson cohort.
506 **(B)** Quantification of absolute bacterial biomass gained (left) and displaced (right) across all gut
507 compartments stratified by taxonomic identity. Values are presented as relative to total Jax^{WT}
508 biomass. **(C)** Absolute bacterial biomass in all gut compartments across mouse cohorts. **(D)**
509 Proportion of bacterial biomass in each gut compartment uniquely found in Envigo donors (Env
510 specific), uniquely found in Jackson Recipients (Jax specific), or observed in both. **(E)** Absolute
511 abundance of select OTUs across gut compartments in Jax^{WT} and Jax^{Env} mouse cohorts.
512
513
514
515
516
517



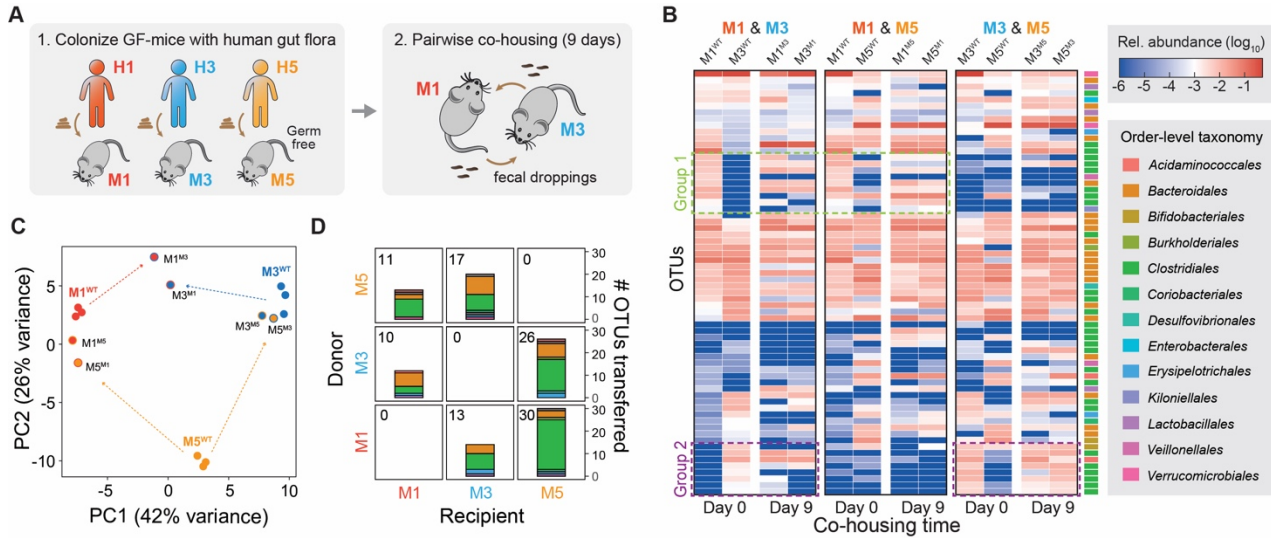
518

Figure 4. FMT results in dramatic restructuring of microbial spatial co-localizations. A-B)
 519 Co-association map indicating significant spatial co-associations amongst native OTUs unique
 520 to **A) Env** and **B) Jax^{WT}** mice. FMT outcomes determined by differential analysis comparing
 521 abundances in Jax^{WT} and Jax^{Env} mice. Rows and columns are clustered using Ward's Linkage. **C)**
 522 Co-association map indicating significant spatial co-associations within the Jax^{Env} microbiota.
 523 OTUs are indicated depending on if they are uniquely found in Env, uniquely found in Jax, or
 524 shared. **D) Sankey diagram** indicating the transfer of OTUs from Jax/Env spatial subgroups to
 525 Jax^{Env} subgroups. **E) Correlation** between the number of observed spatial-associations in the Env
 526 microbiome and engraftment in Jax^{Env} across Env-enriched OTUs. Engraftment Efficiency
 527 indicates the log₂ fold change in abundance comparing Jax^{WT} and Jax^{Env} mice. **F) Number** of
 528 interactions found amongst Env microbes separated by whether they were depleted, unchanged,
 529 or enriched in Jax^{Env} following cohousing (Wilcoxon rank sum test).
 530



531
532 **Figure 5. Envigo microbiota harness unique glycoside hydrolases to metabolize diverse**
533 **carbohydrate substrates. (A)** Number of metagenome-assembled genomes (MAGs) associated
534 with each vendor and their family-level taxonomic distribution. **(B)** Abundance of glycoside
535 hydrolase genes within *Muribaculaceae* MAGs from each vendor. **(C)** OD₆₀₀ Growth assays of
536 fecal communities acquired from Jax^{WT}, Env^{WT}, and Jax^{Env} mice after five days of cohousing.
537 Communities were inoculated in defined minimal media supplemented with single sources of
538 carbohydrates (indicated).

539
540
541
542



543

544 **Figure 6. Humanized mouse microbiomes simulate human FMT outcomes.** (A) Pairwise
545 fecal microbiota (FMT) transfer model of gnotobiotic female C57BL/6 mice harboring 'humanized'
546 microbiomes from individuals spanning the three canonical enterotypes. (B) 16S profiling of
547 mouse fecal communities following nine days of cohousing separated by pairs (N=2 per pair).
548 Clusters 1 & 2 indicate observed microbial transfer events. Rows arranged by hierarchical
549 clustering. (C) PCA of Euclidean distance in OTU composition comparing humanized mice before
550 and after cohousing. The primary label indicates the original mouse microbiome and superscript
551 indicates the cohousing partner. (D) Taxonomic composition of transferred OTUs between
552 C57BL/6 mice harboring 'humanized' microbiomes. The number in the top left indicates the total
553 number of OTUs transferred. OTU color scheme matches (B).

554

555

556

557

558

559

560

561

562

563

564

565

566

567 **RESOURCE AVAILABILITY**

568

569 **Lead contact**

570

571 Further information and requests for resources and reagents should be directed to and will be
572 fulfilled by the lead contact, Harris Wang (hw2429@cumc.columbia.edu).

573

574 **Materials availability**

575

576 This paper does not report original materials.

577

578 **Data and code availability**

- 579 ● Raw sequencing data is available through SRA under BioProject ID: PRJNA1028308.
580 ● Original code and processed datasets are available through
581 https://github.com/gurtecho/Urtecho_et_al_FMT
582 ● Any additional information required to reanalyze the data reported in this paper is available
583 from the lead contact upon request.

584

585 **EXPERIMENTAL MODEL AND SUBJECT DETAILS**

586

587 **Mouse lines**

588

589 C57BL6/J Mice were separately purchased from Jackson Laboratory, Taconic Biosciences,
590 Envigo, and Charles River Laboratories.

591

592 **METHOD DETAILS**

593

594 **Animal procedures.** 6- to 8-week-old female C57BL6/J mice were obtained from different
595 suppliers and allowed to acclimate to the animal facility for a week in cages of four mice. After
596 one week, the bedding was exchanged between cages of mice from the same vendor to normalize
597 their microbiota. To enable FMT by cohousing, after normalization, two mice from each cohort
598 were transferred to a new cage along with two mice from a second cohort. In control groups, all
599 cohoused mice were from the same vendor. Mice were fed Teklad global 18% protein (2018S).

600

601 **Mice feces collection and microbial DNA extraction.** Fresh mouse fecal pellets were collected
602 and kept on dry ice before being weighed and transferring to a -80°C freezer for long-term storage.
603 Whole pellets were suspended in 1 mL PBS and mechanically separated using an inoculating
604 loop. Genomic DNA (gDNA) of fecal microbiota were extracted using a silica bead beating-based
605 protocol adapted from Qiagen MagAttract PowerMicrobiome DNA/RNA Kit [Qiagen 27500-4-EP],
606 detailed fully in Ref⁵⁸. For experiments in which absolute abundance was determined, 1 uL of
607 saturated *Sporosarcina pasteurii* (ATCC 11859) culture was added to the sample prior to bead
608 beating.

609

610 **Luminal Content Collection.** The luminal contents of mice were extracted for 16S and
611 metagenomic sequencing. Mice were euthanized and their intestinal tracts were dissected in a
612 sterile hood. The small intestines were separated into three sections of equal length, and their gut
613 contents as well as those of the cecum and large intestines were extruded into 1.5 mL tubes and
614 transferred to dry ice using forceps. Samples were weighed and processed following the microbial
615 DNA extraction protocol described above.

616

617 **16S rRNA amplicon sequencing.** 16S sequencing of the V4 region for mice gut microbiota was
618 performed using a custom library preparation and sequencing protocol with dual indexing strategy
619 ⁵⁸. Briefly, a 20uL 16S-V4 PCR reaction was set up (1ng extracted gDNA; 1uL forward barcoded
620 P5 primer; 1uL reverse barcoded P7 primer; 10uL NEBNext® Ultra™ II Q5® Master Mix [NEB
621 M0544X]; SYBR Green I at 0.2x final concentration) and subjected to a quantitative amplification
622 on a thermal cycler (98°C 30s; cycles: 98°C 10s, 55°C 20s, 65°C 60s; 65°C 5min; 4°C infinite).
623 PCR reaction was stopped during exponential phase to avoid amplification bias (typically 13-16
624 cycles) and the cycling was skipped to the final extension step. Next, 16S-V4 amplicon libraries
625 were pooled based on the fluorescence increase at the last cycle and subjected to gel
626 electrophoresis. DNA bands at ~390bp were excised from gel and purified using Wizard™ SV
627 Gel and PCR Cleanup System (Promega A9282) following the manufacturer's instructions.
628 Purified libraries were sequenced on Illumina MiSeq platform (reagent kits: v2 300-cycles, paired-
629 end mode) at 8 pM loading concentration with 25% PhiX spike-in (Illumina FC-110-3001). Custom
630 sequencing primers were spiked into reagent cartridge (well 12: 16SV4_read1, well 13:
631 16SV4_index1, well 14: 16SV4_read2) following the manufacturer's instructions.

632

633 **16S rRNA amplicon analysis and OTU clustering.** Raw sequencing reads of 16SV4 amplicon
634 were analyzed by USEARCH v11.0.667⁵⁹. Specifically, paired-end reads were merged using “-

635 fastq_mergepairs" mode with default setting. Merged reads were then subjected to quality filtering
636 using "-fastq_filter" mode with the option "-fastq_maxee 1.0 -fastq_minlen 240" to only keep reads
637 with less than 1 expected error base and greater than 240bp. Remaining reads were deduplicated
638 (-fastx_uniques) and clustered into OTUs (-unoise3) at 100% identity, and merged reads were
639 then searched against OTU sequences (-otutab) to generate OTU count tables. Taxonomy of
640 OTUs were assigned using the Ribosomal Database Project classifier trained with 16S rRNA
641 training set 16.

642

643 **OTU Filtering and Count Normalization.** OTU count tables were normalized to relative or
644 absolute abundance and filtered by relative abundance for downstream analyses as follows. For
645 experiments lacking spike-in controls, reads were normalized by relative abundance within each
646 sample and OTUs with a relative abundance below 0.5% (averaged across biological replicates)
647 were removed. Absolute abundance measurements were determined by normalizing relative
648 abundance of all OTUs to spike-in OTU counts as well as the weight of the fecal pellet.

649

650 **Shotgun metagenome sequencing.** Library preparation of shotgun metagenome sequencing
651 was performed using the same gDNA used for 16SV4 amplicon sequencing. Briefly, Nextera
652 libraries were prepared following a scale-down Tn5 tagmentation-based library preparation
653 protocol with 2ng gDNA as input⁶⁰. Libraries were sequenced on Illumina Nextseq 500/550
654 platform (2 x 75bp) and HiSeq platform (2 × 150bp) following the manufacturer's instructions.

655

656 **Metagenome assembly and binning.** Raw reads of shotgun metagenome sequencing were
657 processed by Cutadaptv2.1^{61,62} with the following parameters "--minimum-length 25:25 -u 5 -U 5
658 -q 15 --max-n 0 --pair-filter=any" to remove Nextera adapters and low-quality bases. To obtain
659 metagenome-assembled genomes (MAGs), processed raw reads of each mouse cohort were first
660 assembled using metaSPAdes v3.11.1⁶³ with default parameters. Yielding contigs of each cohort
661 were split into 10kb fragments to denoise assembly artifacts and then subjected to binning by
662 MaxBin v2.2.6^{63,64}, MetaBAT v2.12.1⁶⁵, CONCOCT v1.0.0^{65,66}, and MyCC⁶⁷ (no version info) with
663 default settings. Results from different tools were further integrated and corrected by DAS Tool
664 v.1.1.1⁶⁸ to generate a first round of metagenome bins. Raw reads were then aligned to
665 metagenome bins using Bowtie2 v2.3.4⁶⁹ in "—very-sensitive" mode and partitioned into bins
666 based on alignments. Next, partitioned reads of each bin were assembled separately by Unicycler
667 v.0.4.4⁷⁰ with default setting to generate final MAGs. All MAGs were then evaluated for quality

668 and contamination by Quast v4.6.3⁷¹ and CheckM v1.0.13⁷² and subsequently subjected to
669 taxonomy annotation by GTDB-Tk v1.7.0^{72,73}.

670

671 **Functional annotation of MAGs.** Protein sequences of MAGs were annotated by Prokka v1.12⁷⁴
672 with default settings and were used for functional annotation to assign CAZyme and KEGG terms.
673 Briefly, reference protein sequences with specific CAZyme annotation or KEGG Orthology terms
674 were downloaded from CAZyme database or KEGG database respectively, and homolog search
675 was performed for MAG protein sequences against reference sequences using BLASTP v2.9.0+
676 with maximum targets no more than 50. BLAST targets with e-value < 0.0001 were considered
677 as hits, and the CAZyme or KEGG Orthology terms annotation was then assigned to MAGs'
678 protein sequences based on their BLAST hits.

679

680 **MaPS-Seq Sample Collection.** Fresh fecal pellets were collected and immediately transferred
681 to tubes containing methacarn (60% methanol, 30% chloroform, 10% acetic acid). After 24 hrs of
682 fixation, samples were transferred to 70% ethanol and stored at 4°C until use. Samples were
683 processed following the MaPS-Seq protocol⁴³. After fracturing and barcoding, 20-40 micron
684 particles were isolated by size-exclusion filtering for sequencing. For each mouse, two technical
685 replicates of approximately 20,000 particles were used for sequencing. Samples were sequenced
686 on an Illumina NextSeq550 (2 x 250 bp).

687

688 **MaPS-Seq Particle Clustering.** particles were clustered using the louvain algorithm, as
689 implemented in the Seurat R package function FindClusters() with the resolution parameter set
690 to 0.5.

691

692 **Spatial association analysis within MaPS-Seq Particles.** A frequentist analysis was performed
693 to identify spatial associations between OTUs. Briefly, OTU counts in each particle were binarized
694 to create a matrix representing the presence or absence of each OTU in each particle. To simulate
695 a null model of co-occurrence, we used the EcoSimR package v0.1.0 to randomly shuffle
696 presence and absence counts and count the number of particles each OTU pair was found
697 together for. This was performed 1000 times for each sample to generate a distribution of co-
698 occurrence frequencies for each OTU pair. We then determined where the observed co-
699 occurrence frequency laid along this distribution and calculated the corresponding Z-score and
700 two-tailed P-value. P-values were adjusted using false-discovery rate and an adjusted p-value <

701 0.05 was considered significant. Network analysis was performed in R using the packages ggraph
702 v2.0 and igraph v1.3.1 using co-occurrence Z-scores to indicate the magnitude of relationships.

703

704 **Polysaccharide Utilization Growth Assays.** Fecal communities were grown in Bacteroides
705 minimal media⁷⁵ cultures supplemented with various polysaccharides. Fecal pellets were
706 mechanically separated in 1 mL PBS and diluted 1:10 in PBS before being inoculated in a 96-well
707 culture for a total dilution rate of 1:400. Cultures were supplemented with 10 mg/mL of a single
708 carbohydrate. The resulting inoculated cultures were grown over 48 hrs in a Biotek Powerwave
709 XS plate reader (product code: B-PWXS) taking OD₆₀₀ measurements every 15 minutes and the
710 data was exported for analysis in R.

711

712 **Ethical review.** This study was approved and conducted under Columbia University Medical
713 Center Institutional Animal Care and Use Committee (Protocol #AC-AABD4551) and complied
714 with all relevant regulations.

715

716 **Acknowledgements**

717 We thank members of the Wang laboratory for advice and comments on the manuscript. H.H.W.
718 acknowledges funding support from the NSF (MCB-2025515), NIH (1R01AI132403,
719 1R01DK118044, 1R21AI146817), ONR (N00014-18-1-2237, N00014-17-1-2353), Burroughs
720 Wellcome Fund (1016691), Irma T. Hirschl Trust, and Schaefer Research Award. G.U. was
721 supported by the HHMI Hanna H. Gray Postdoctoral Fellowship (GT15182). T.M. is supported by
722 NIH Medical Scientist Training Program (T32GM007367). R.U.S. was supported by a Fannie and
723 John Hertz Foundation Fellowship and an NSF Graduate Research Fellowship (DGE-1644869).
724 M.R. and F.V.C. are supported by NSF Graduate Research Fellowships (DGE-1644869). G.K.G.
725 acknowledges funding support from the NSF (MCB-2025515), NIH (1R01GM130777), and BWH
726 President's Scholar Award.

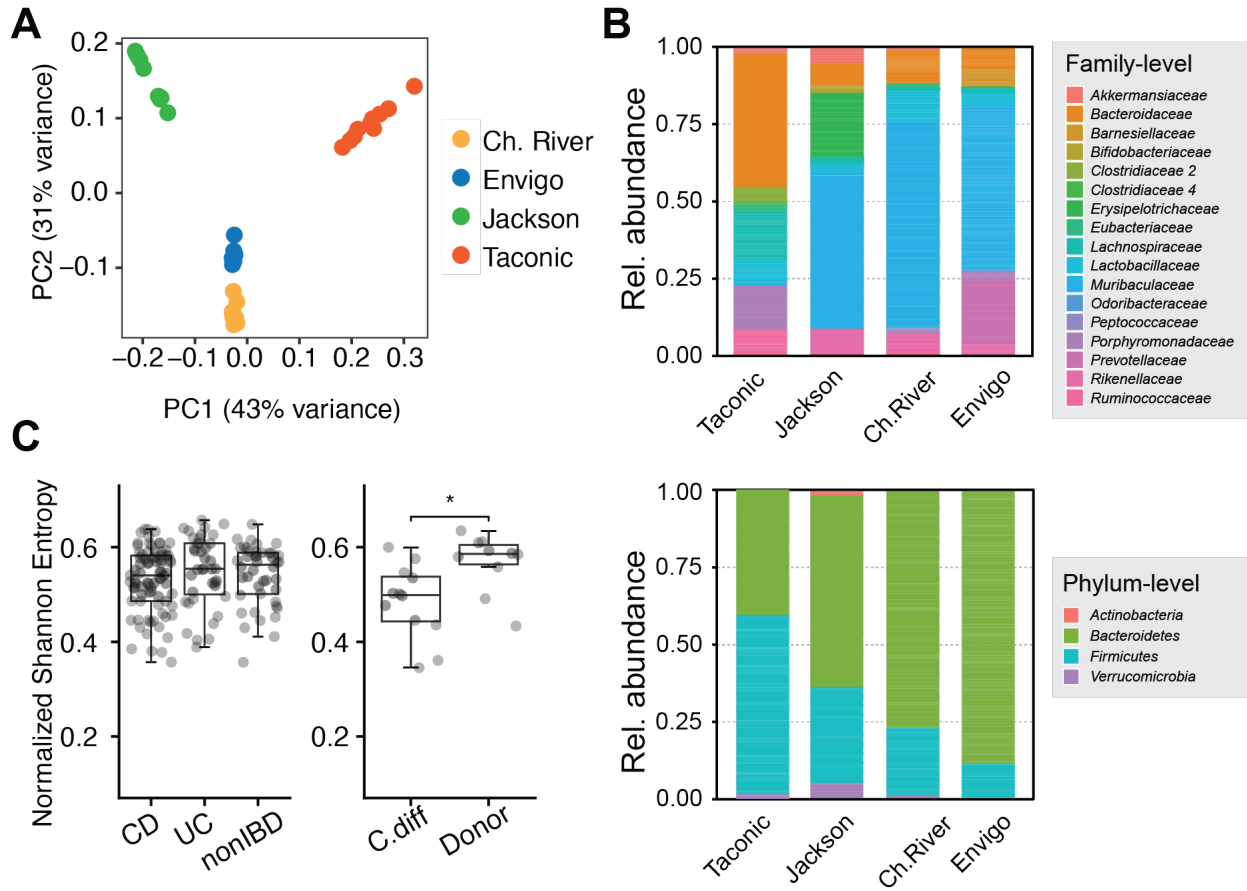
727

728 **Declaration of Interests**

729 H.H.W. is a scientific advisor of SNIPR Biome, Kingdom Supercultures, Fitbiomics, Arranta Bio,
730 VecX Biomedicines, Genus PLC and a scientific cofounder of Aclid, all of whom are not involved
731 in the study. R.U.S is a cofounder of Kingdom Supercultures. All the other authors declare no
732 competing interests.

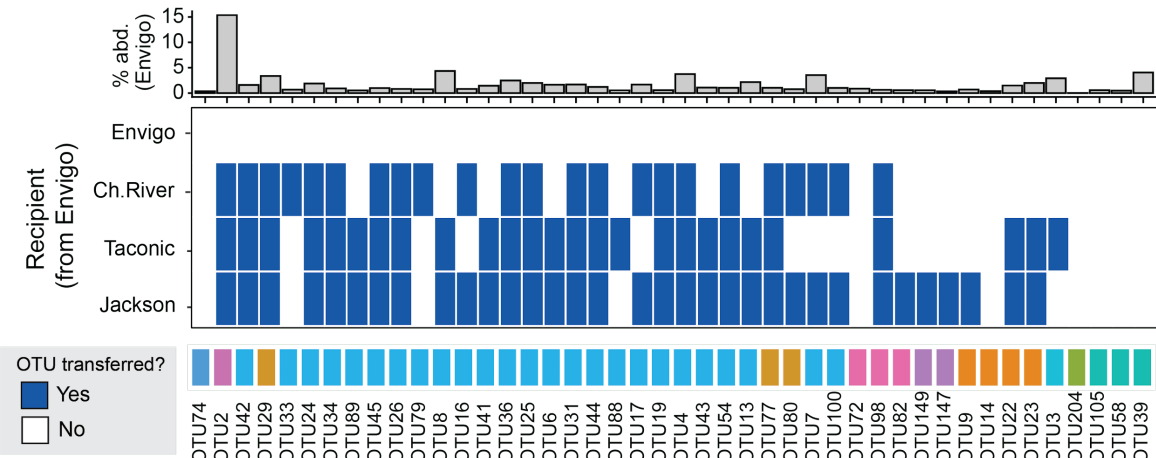
733

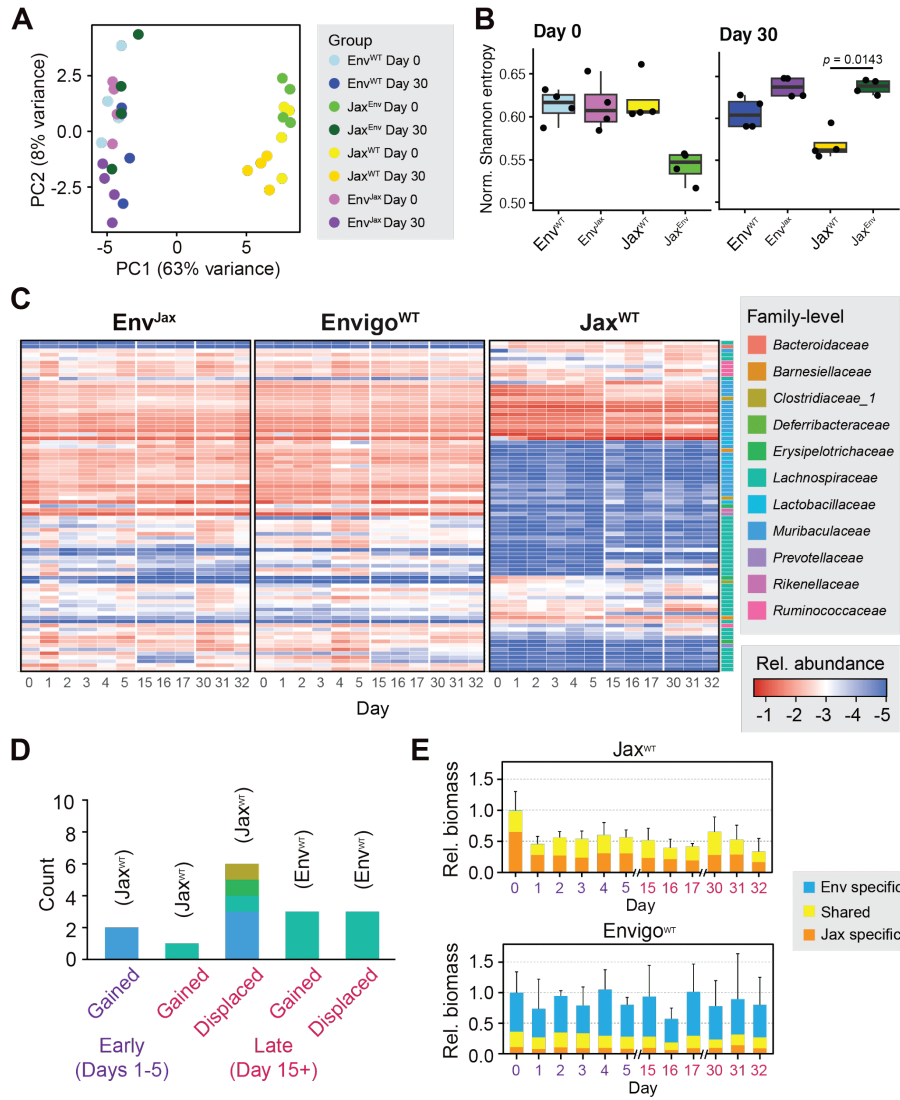
734



735
736
737
738
739
740
741
742
743
744
745
746
747
748

Supplementary Figure 1. Microbiome OTU composition and functional annotations. (A) PCA of unweighted UniFrac distance comparing mouse 16S profiles from different vendors (B) Family-level (top) and Phylum-level (bottom) 16S composition of microbiomes from various vendors. (C) Shannon Diversity estimations of human fecal 16S profiles from healthy (non-IBD, Donor) and diseased ($p = 0.01377$, Wilcoxon rank sum test) (UC: Ulcerative Colitis, CD: Crohn's Disease, C.diff: *Clostridioides difficile*) cohorts. IBD – Irritable Bowel Disease; UC – Ulcerative Colitis; CD – *Clostridioides difficile*.

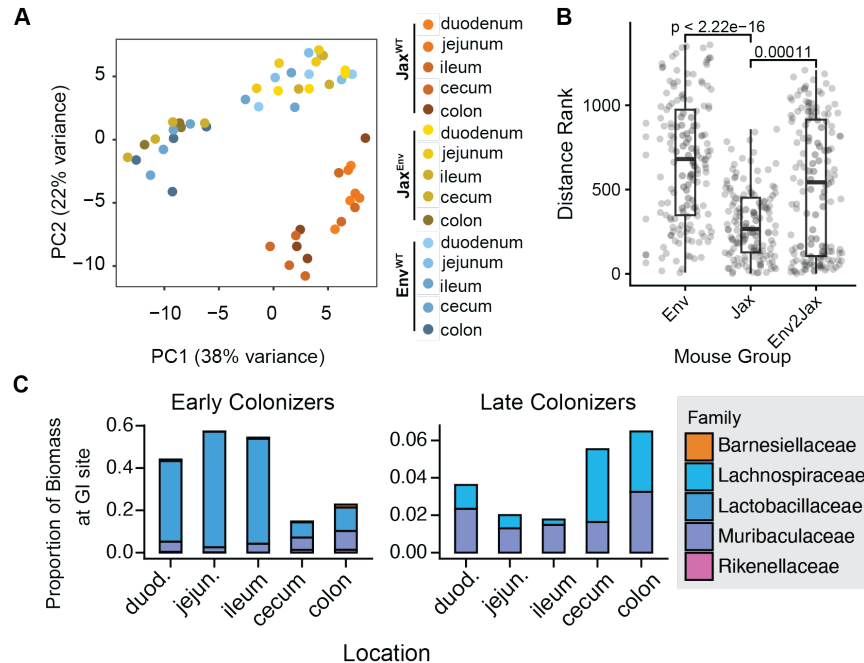




761

762 **Supplementary Figure 3. (A)** PCA of 16S fecal microbiome composition between mouse cohorts
 763 at days 0 and day 30 of cohousing. **(B)** Shannon Diversity Index (SDI) of cohoused mice at day
 764 0 and day 30 ($N = 4$). **(C)** Longitudinal 16S microbiome profiling of cohoused mice controls. (left)
 765 Envigo mice cohoused with Jackson mice, (middle) Envigo mice cohoused with other Envigo
 766 mice, (right) Jackson mice cohoused with other Jackson mice ($N = 4$). **(D)** OTU composition of
 767 microbes gained and lost during cohousing in non-mixed Jax^{WT} mouse controls and Env^{WT} mouse
 768 controls. **(E)** Relative bacterial biomass within feces of (top) Jax^{WT} mice non-mixed controls and
 769 (bottom) Env^{WT} mouse non-mixed controls. Biomass is colored by whether OTUs are uniquely
 770 found in microbiomes of Envigo donors (Env specific), uniquely found in Jackson Recipients (Jax
 771 specific), or observed in both (Shared).

772



773

774 **Supplementary Figure 4. A)** PCA of 16S microbiome composition across different gut
 775 compartments ($N = 4$). Jax^{Env} mice have greater variance between compartments and resemble
 776 the Env^{WT}. **B)** Analysis of Similarities (ANOSIM) measurement of dissimilarity within mouse
 777 groups (Wilcoxon rank sum test). **C)** Relative proportion of Jax^{Env} mouse microbiome composed
 778 of (left) Early and (right) late colonizing OTUs at each GI site after cohousing. Sampling done at
 779 day 32 of mouse cohousing.

780

781

782

783

784

785

786

787

788

789

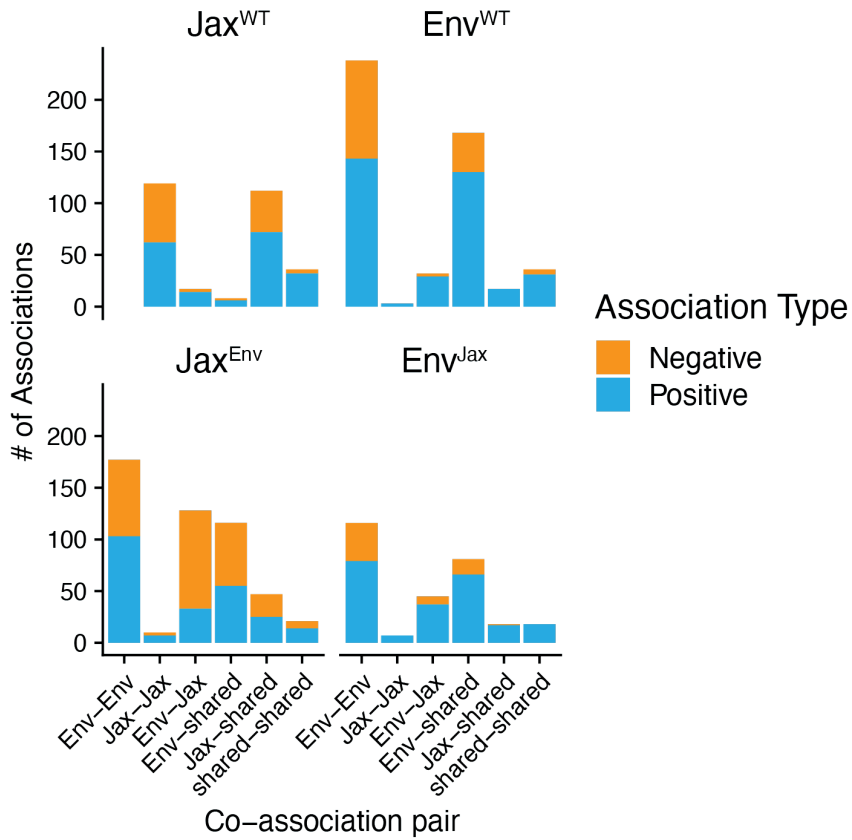
790

791

792

793

794



795

796 **Supplementary Figure 5**, related to **Figure 4. Number of interactions between different types**
 797 **of microbial pairs**. Microbes were considered shared if they exhibited greater than 0.5%
 798 abundance in both Jax^{WT} and Env^{WT} populations whereas Env^{WT} and Jax^{WT} OTUs were only
 799 above this threshold in one of these groups. While Jax^{WT} contained many Jax-Jax spatial
 800 associations, relatively few were observed in Jax^{Env}. Instead, Jax microbiota formed interactions
 801 with Env (Env-Jax) and Shared (Jax-shared) microbiota.

802

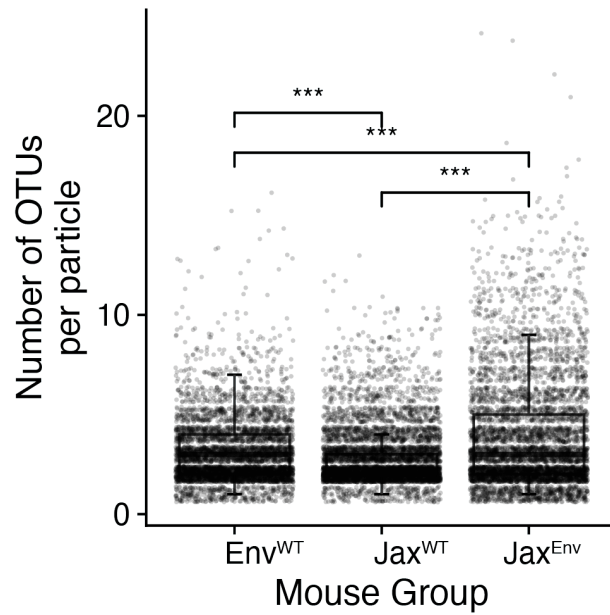
803

804

805

806

807



808

809 **Supplementary Figure 6**, related to **Figure 4**. Number of distinct OTUs identified within particles
810 derived from Env, Jax^{Env}, and Jax^{WT} mice. Env mean: 3.01, Jax^{Env} mean: 3.76, Jax^{WT} mean: 2.88
811 (** = $p < 0.001$, Wilcoxon rank-sum test).

812

813

814

815

816

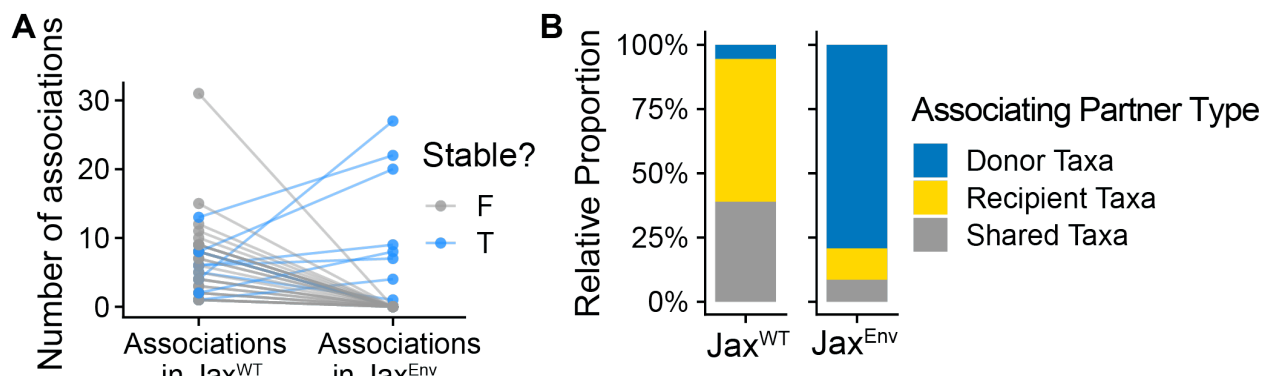
817

818

819

820

821



822

Supplementary Figure 7, related to Figure 4. Jax OTU interactions in native and donor microbiomes. **(A)** Number of associations by Jax OTUs in Jax^{WT} mice and Jax^{Env} mice. Stable Jax microbiota show an increase in the number of associations they engage in post-FMT. **(B)** Composition of associating partners by Jax OTUs in Jax^{WT} mice and Jax^{Env} mice. Stable Jax microbiota establish spatial associations with donor taxa post-FMT.

823

824

825

826

827

828

829

830

831

832

833

834

835

836

837

838

839

840

841

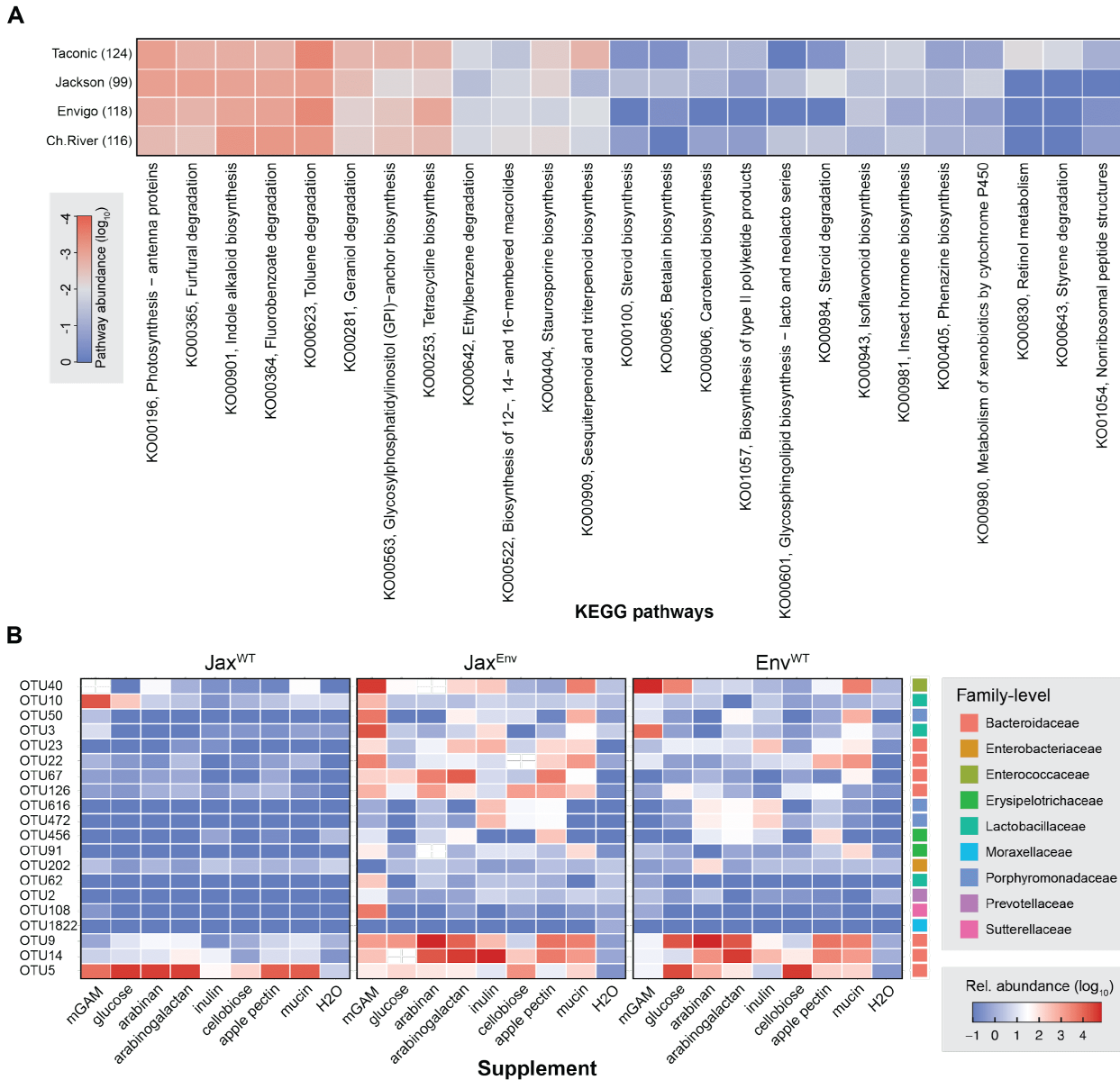
842

843

844

845

846



847

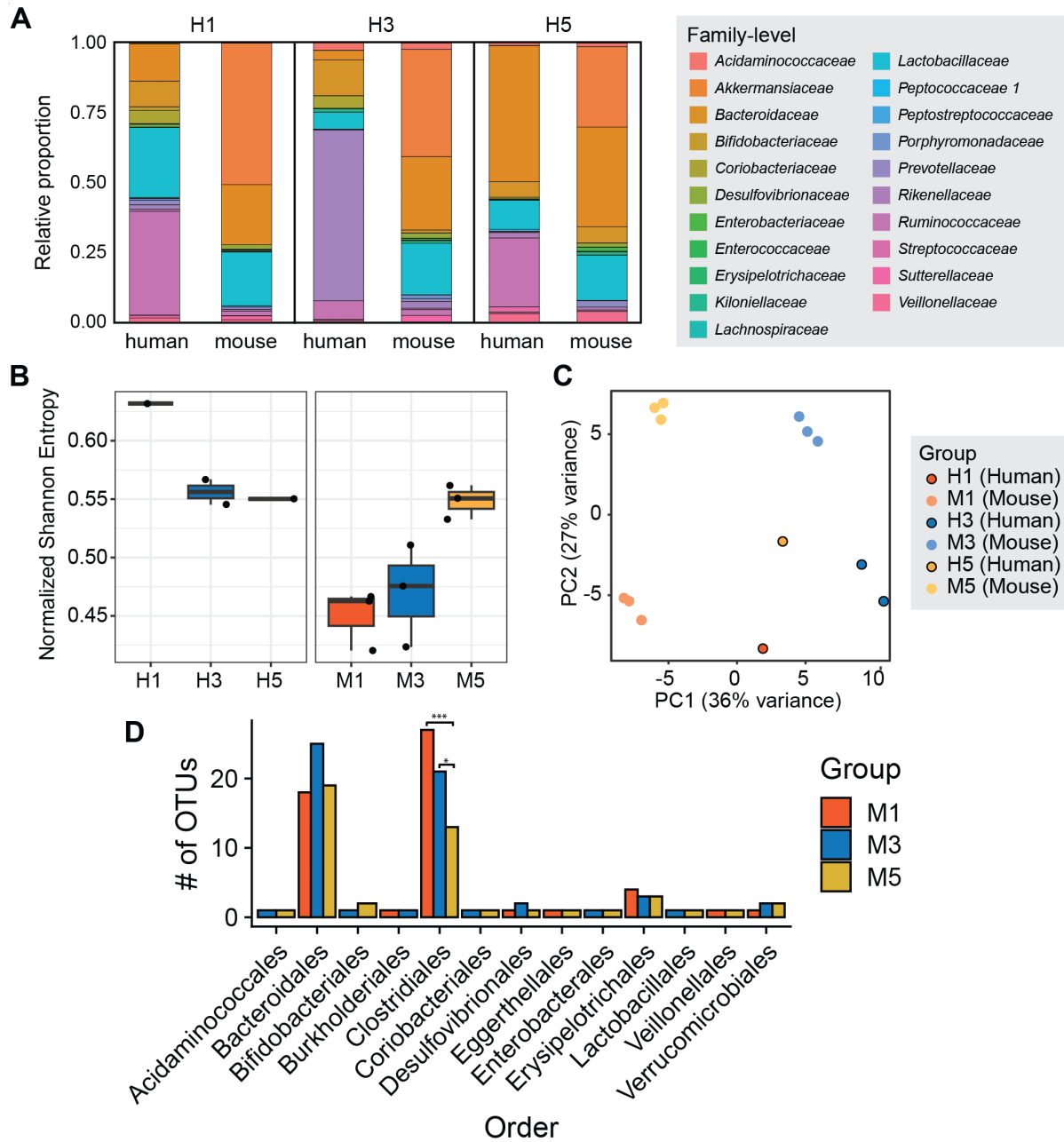
848 **Supplementary Figure 8. 16S profiling of fecal microbiome communities after culturing.**

849 **(A)** Abundance of KEGG-annotated pathways identified amongst MAGs from each mouse
 850 vendor. Pathways presented exhibited the greatest variability between microbiomes. **(B)** Fecal
 851 communities were inoculated into *Bacteroides* minimal media supplemented with the indicated
 852 carbohydrate sources. Post FMT fecal pellets were harvested after five days of cohousing
 853 Jackson mice with Envigo.

854

855

856



857

858 **Supplementary Figure 9. 16S profiling of human donors and humanized mice.** **A)** Family-
 859 level OTU composition of human fecal donors and corresponding humanized mice. Two sampling
 860 replicates were performed for human H3. **B)** Normalized Shannon Entropy of (left) human fecal
 861 donors and (right) humanized mice ($N = 3$ / donor). **C)** PCA of microbiome composition between
 862 human donors and humanized mouse cohorts at day 0 prior to mouse cohousing. **D)** Number of
 863 OTUs corresponding to each species in humanized mouse microbiomes. M1 and M3 mice contain
 864 significantly more *Clostridiales* OTUs than M5. (Wilcoxon rank sum test, M1-M5: $p = 0.00074$,
 865 M3-M5: $p = 0.027$).

866 REFERENCES

- 867 1. Lynch, S. V. & Pedersen, O. The Human Intestinal Microbiome in Health and Disease. *N.
868 Engl. J. Med.* **375**, 2369–2379 (2016).
- 869 2. Chiu, L. *et al.* Protective Microbiota: From Localized to Long-Reaching Co-Immunity. *Front.
870 Immunol.* **0**, (2017).
- 871 3. Martin, A. M., Sun, E. W., Rogers, G. B. & Keating, D. J. The Influence of the Gut
872 Microbiome on Host Metabolism Through the Regulation of Gut Hormone Release. *Front.
873 Physiol.* **0**, (2019).
- 874 4. Wernroth, M.-L. *et al.* Development of gut microbiota during the first 2 years of life. *Sci.
875 Rep.* **12**, 9080 (2022).
- 876 5. Kim, S., Covington, A. & Pamer, E. G. The intestinal microbiota: Antibiotics, colonization
877 resistance, and enteric pathogens. *Immunol. Rev.* **279**, 90–105 (2017).
- 878 6. Faintuch, J. & Faintuch, S. *Microbiome and Metabolome in Diagnosis, Therapy, and other
879 Strategic Applications.* (Academic Press, 2019).
- 880 7. Bucci, V. *et al.* MDSINE: Microbial Dynamical Systems INference Engine for microbiome
881 time-series analyses. *Genome Biol.* **17**, 121 (2016).
- 882 8. Lee, J.-Y., Tsolis, R. M. & Bäumler, A. J. The microbiome and gut homeostasis. *Science*
883 **377**, eabp9960 (2022).
- 884 9. Olsson, L. M. *et al.* Dynamics of the normal gut microbiota: A longitudinal one-year
885 population study in Sweden. *Cell Host Microbe* **30**, 726–739.e3 (2022).
- 886 10. Rakoff-Nahoum, S., Coyne, M. J. & Comstock, L. E. An ecological network of
887 polysaccharide utilization among human intestinal symbionts. *Curr. Biol.* **24**, 40–49 (2014).
- 888 11. Flint, H. J., Scott, K. P., Duncan, S. H., Louis, P. & Forano, E. Microbial degradation of
889 complex carbohydrates in the gut. *Gut Microbes* **3**, 289–306 (2012).
- 890 12. Sung, J. *et al.* Global metabolic interaction network of the human gut microbiota for context-

- 891 specific community-scale analysis. *Nat. Commun.* **8**, 15393 (2017).
- 892 13. Marion, S. *et al.* Biogeography of microbial bile acid transformations along the murine gut.
- 893 *J. Lipid Res.* **61**, 1450–1463 (2020).
- 894 14. Scales, B. S., Dickson, R. P. & Huffnagle, G. B. A tale of two sites: how inflammation can
- 895 reshape the microbiomes of the gut and lungs. *J. Leukoc. Biol.* **100**, 943–950 (2016).
- 896 15. Venturelli, O. S. *et al.* Deciphering microbial interactions in synthetic human gut microbiome
- 897 communities. *Mol. Syst. Biol.* **14**, e8157 (2018).
- 898 16. Lozupone, C. A., Stombaugh, J. I., Gordon, J. I., Jansson, J. K. & Knight, R. Diversity,
- 899 stability and resilience of the human gut microbiota. *Nature* **489**, 220–230 (2012).
- 900 17. Khanna, S. Microbiota Replacement Therapies: Innovation in Gastrointestinal Care. *Clin.*
- 901 *Pharmacol. Ther.* **103**, 102–111 (2018).
- 902 18. Ianiro, G. *et al.* Variability of strain engraftment and predictability of microbiome
- 903 composition after fecal microbiota transplantation across different diseases. *Nat. Med.* **28**,
- 904 1913–1923 (2022).
- 905 19. Wilson, B. C., Vatanen, T., Cutfield, W. S. & O’Sullivan, J. M. The Super-Donor
- 906 Phenomenon in Fecal Microbiota Transplantation. *Front. Cell. Infect. Microbiol.* **9**, (2019).
- 907 20. Smillie, C. S. *et al.* Strain Tracking Reveals the Determinants of Bacterial Engraftment in
- 908 the Human Gut Following Fecal Microbiota Transplantation. *Cell Host Microbe* **23**, 229–
- 909 240.e5 (2018).
- 910 21. Vermeire, S. *et al.* Donor Species Richness Determines Faecal Microbiota Transplantation
- 911 Success in Inflammatory Bowel Disease. *J. Crohns. Colitis* **10**, 387–394 (2015).
- 912 22. Podlesny, D. *et al.* Identification of clinical and ecological determinants of strain
- 913 engraftment after fecal microbiota transplantation using metagenomics. *Cell Rep Med* **3**,
- 914 100711 (2022).
- 915 23. Schmidt, T. S. B. *et al.* Drivers and determinants of strain dynamics following fecal
- 916 microbiota transplantation. *Nat. Med.* **28**, 1902–1912 (2022).

- 917 24. The Integrative Human Microbiome Project. *Nature* **569**, 641–648 (2019).
- 918 25. Velazquez, E. M. *et al.* Endogenous Enterobacteriaceae underlie variation in susceptibility
919 to *Salmonella* infection. *Nature Microbiology* **4**, 1057–1064 (2019).
- 920 26. Wolff, N. S. *et al.* Vendor effects on murine gut microbiota and its influence on
921 lipopolysaccharide-induced lung inflammation and Gram-negative pneumonia. *Intensive
922 Care Medicine Experimental* **8**, 1–13 (2020).
- 923 27. Ericsson, A. C. *et al.* Effects of Vendor and Genetic Background on the Composition of the
924 Fecal Microbiota of Inbred Mice. *PLoS One* **10**, e0116704 (2015).
- 925 28. Lloyd-Price, J. *et al.* Multi-omics of the gut microbial ecosystem in inflammatory bowel
926 diseases. *Nature* **569**, 655–662 (2019).
- 927 29. Weingarden, A. *et al.* Dynamic changes in short- and long-term bacterial composition
928 following fecal microbiota transplantation for recurrent *Clostridium difficile* infection.
929 *Microbiome* **3**, 1–8 (2015).
- 930 30. Bokoliya, S. C., Dorsett, Y., Panier, H. & Zhou, Y. Procedures for Fecal Microbiota
931 Transplantation in Murine Microbiome Studies. *Front. Cell. Infect. Microbiol.* **0**, (2021).
- 932 31. Ericsson, A. C., Personett, A. R., Turner, G., Dorfmeyer, R. A. & Franklin, C. L. Variable
933 Colonization after Reciprocal Fecal Microbiota Transfer between Mice with Low and High
934 Richness Microbiota. *Front. Microbiol.* **8**, 196 (2017).
- 935 32. Seedorf, H. *et al.* Bacteria from Diverse Habitats Colonize and Compete in the Mouse Gut.
936 *Cell* **159**, 253–266 (2014).
- 937 33. Li, W. *et al.* A Cross-Scale Neutral Theory Approach to the Influence of Obesity on
938 Community Assembly of Human Gut Microbiome. *Front. Microbiol.* **0**, (2018).
- 939 34. Sloan, W. T. *et al.* Quantifying the roles of immigration and chance in shaping prokaryote
940 community structure. *Environ. Microbiol.* **8**, 732–740 (2006).
- 941 35. Donaldson, G. P., Lee, S. M. & Mazmanian, S. K. Gut biogeography of the bacterial
942 microbiota. *Nat. Rev. Microbiol.* **14**, 20–32 (2015).

- 943 36. Tropini, C., Earle, K. A., Huang, K. C. & Sonnenburg, J. L. The Gut Microbiome:
944 Connecting Spatial Organization to Function. *Cell Host Microbe* **21**, 433–442 (2017).
- 945 37. Turnbaugh, P. J. *et al.* The effect of diet on the human gut microbiome: a metagenomic
946 analysis in humanized gnotobiotic mice. *Sci. Transl. Med.* **1**, 6ra14 (2009).
- 947 38. Zmora, N. *et al.* Personalized Gut Mucosal Colonization Resistance to Empiric Probiotics Is
948 Associated with Unique Host and Microbiome Features. *Cell* **174**, 1388–1405.e21 (2018).
- 949 39. Somerfield, Paul J., K. Robert Clarke, and Ray N. Gorley. "A generalised analysis of
950 similarities (ANOSIM) statistic for designs with ordered factors." *Austral Ecology* 46, no. 6
951 (2021): 901-910.
- 952 40. Hu, J. *et al.* Gut microbiota-mediated secondary bile acids regulate dendritic cells to
953 attenuate autoimmune uveitis through TGR5 signaling. *Cell Rep.* **36**, (2021).
- 954 41. Ridlon, J. M., Wolf, P. G. & Gaskins, H. R. Taurocholic acid metabolism by gut microbes
955 and colon cancer. *Gut Microbes* **7**, 201–215 (2016).
- 956 42. Hibbing, M. E., Fuqua, C., Parsek, M. R. & Peterson, S. B. Bacterial competition: surviving
957 and thriving in the microbial jungle. *Nat. Rev. Microbiol.* **8**, 15–25 (2009).
- 958 43. Sheth, R. U. *et al.* Spatial metagenomic characterization of microbial biogeography in the
959 gut. *Nat. Biotechnol.* **37**, 877–883 (2019).
- 960 44. Gotelli, N. J. & Ulrich, W. The empirical Bayes approach as a tool to identify non-random
961 species associations. *Oecologia* **162**, 463–477 (2010).
- 962 45. Kearney, S. M., Gibbons, S. M., Erdman, S. E. & Alm, E. J. Orthogonal Dietary Niche
963 Enables Reversible Engraftment of a Gut Bacterial Commensal. *Cell Rep.* **24**, 1842–1851
964 (2018).
- 965 46. Shepherd, E. S., DeLoache, W. C., Pruss, K. M., Whitaker, W. R. & Sonnenburg, J. L. An
966 exclusive metabolic niche enables strain engraftment in the gut microbiota. *Nature* **557**,
967 (2018).
- 968 47. Arumugam, M. *et al.* Enterotypes of the human gut microbiome. *Nature* **473**, 174–180

- 969 (2011).
- 970 48. Park, J. C. & Im, S.-H. Of men in mice: the development and application of a humanized
971 gnotobiotic mouse model for microbiome therapeutics. *Exp. Mol. Med.* **52**, 1383–1396
972 (2020).
- 973 49. Koenig, J. E. *et al.* Succession of microbial consortia in the developing infant gut
974 microbiome. *Proc. Natl. Acad. Sci. U. S. A.* **108 Suppl 1**, 4578–4585 (2011).
- 975 50. Ng, K. M. *et al.* Recovery of the Gut Microbiota after Antibiotics Depends on Host Diet,
976 Community Context, and Environmental Reservoirs. *Cell Host Microbe* **28**, 628 (2020).
- 977 51. Martínez, I. *et al.* Experimental evaluation of the importance of colonization history in early-
978 life gut microbiota assembly. (2018) doi:10.7554/eLife.36521.
- 979 52. Levy, R. *et al.* Longitudinal analysis reveals transition barriers between dominant ecological
980 states in the gut microbiome. *Proc. Natl. Acad. Sci. U. S. A.* **117**, 13839–13845 (2020).
- 981 53. Rowland, I. *et al.* Gut microbiota functions: metabolism of nutrients and other food
982 components. *Eur. J. Nutr.* **57**, 1–24 (2018).
- 983 54. Frazier, K. & Chang, E. B. Intersection of the Gut Microbiome and Circadian Rhythms in
984 Metabolism. *Trends Endocrinol. Metab.* **31**, 25–36 (2020).
- 985 55. Liao, J. *et al.* The importance of neutral and niche processes for bacterial community
986 assembly differs between habitat generalists and specialists. *FEMS Microbiol. Ecol.* **92**,
987 fiw174 (2016).
- 988 56. Watson, A. R. *et al.* Metabolic independence drives gut microbial colonization and
989 resilience in health and disease. *Genome Biol.* **24**, 78 (2023).
- 990 57. Button, J. E. *et al.* Dosing a synbiotic of human milk oligosaccharides and *B. infantis* leads
991 to reversible engraftment in healthy adult microbiomes without antibiotics. *Cell Host
992 Microbe* **30**, 712–725.e7 (2022).
- 993 58. Ji, B. W. *et al.* Quantifying spatiotemporal variability and noise in absolute microbiota
994 abundances using replicate sampling. *Nat. Methods* **16**, 731–736 (2019).

- 995 59. Edgar, R. C. Search and clustering orders of magnitude faster than BLAST. *Bioinformatics*
996 **26**, 2460–2461 (2010).
- 997 60. Baym, M. *et al.* Inexpensive Multiplexed Library Preparation for Megabase-Sized Genomes.
998 *PLoS One* **10**, e0128036 (2015).
- 999 61. Martin, M. Cutadapt removes adapter sequences from high-throughput sequencing reads.
1000 *EMBnet.journal* **17**, 10–12 (2011).
- 1001 62. Maki, K. A., Wolff, B., Varuzza, L., Green, S. J. & Barb, J. J. Multi-amplicon microbiome
1002 data analysis pipelines for mixed orientation sequences using QIIME2: Assessing reference
1003 database, variable region and pre-processing bias in classification of mock bacterial
1004 community samples. *PLoS One* **18**, e0280293 (2023).
- 1005 63. Nurk, S., Meleshko, D., Korobeynikov, A. & Pevzner, P. A. metaSPAdes: a new versatile
1006 metagenomic assembler. *Genome Res.* **27**, 824–834 (2017).
- 1007 64. Wu, Y.-W., Tang, Y.-H., Tringe, S. G., Simmons, B. A. & Singer, S. W. MaxBin: an
1008 automated binning method to recover individual genomes from metagenomes using an
1009 expectation-maximization algorithm. *Microbiome* **2**, 26 (2014).
- 1010 65. Kang, D. D. *et al.* MetaBAT 2: an adaptive binning algorithm for robust and efficient
1011 genome reconstruction from metagenome assemblies. *PeerJ* **7**, e7359 (2019).
- 1012 66. Alneberg, J. *et al.* Binning metagenomic contigs by coverage and composition. *Nat.*
1013 *Methods* **11**, 1144–1146 (2014).
- 1014 67. Lin, H.-H. & Liao, Y.-C. Accurate binning of metagenomic contigs via automated clustering
1015 sequences using information of genomic signatures and marker genes. *Sci. Rep.* **6**, 24175
1016 (2016).
- 1017 68. Sieber, C. M. K. *et al.* Recovery of genomes from metagenomes via a dereplication,
1018 aggregation and scoring strategy. *Nature Microbiology* **3**, 836–843 (2018).
- 1019 69. Langmead, B. & Salzberg, S. L. Fast gapped-read alignment with Bowtie 2. *Nat. Methods*
1020 **9**, 357–359 (2012).

- 1021 70. Wick, R. R., Judd, L. M., Gorrie, C. L. & Holt, K. E. Unicycler: Resolving bacterial genome
1022 assemblies from short and long sequencing reads. *PLoS Comput. Biol.* **13**, e1005595
1023 (2017).
- 1024 71. Gurevich, A., Saveliev, V., Vyahhi, N. & Tesler, G. QUAST: quality assessment tool for
1025 genome assemblies. *Bioinformatics* **29**, 1072–1075 (2013).
- 1026 72. Parks, D. H., Imelfort, M., Skennerton, C. T., Hugenholtz, P. & Tyson, G. W. CheckM:
1027 assessing the quality of microbial genomes recovered from isolates, single cells, and
1028 metagenomes. *Genome Res.* **25**, 1043–1055 (2015).
- 1029 73. Chaumeil, P.-A., Mussig, A. J., Hugenholtz, P. & Parks, D. H. GTDB-Tk: a toolkit to classify
1030 genomes with the Genome Taxonomy Database. *Bioinformatics* **36**, 1925–1927 (2019).
- 1031 74. Seemann, T. Prokka: rapid prokaryotic genome annotation. *Bioinformatics* **30**, 2068–2069
1032 (2014).
- 1033 75. Bacic, M. K. & Smith, C. J. Laboratory maintenance and cultivation of bacteroides species.
1034 *Curr. Protoc. Microbiol. Chapter 13*, Unit 13C.1 (2008).

1035